

1  
2  
3  
4 **Measurement Report: Interpretation of Wide Range**  
5 **Particulate Matter Size Distributions in Delhi**  
6

7 **Ülkü Alver Şahin<sup>1</sup>, Roy M Harrison<sup>2,a</sup>, Mohammed S. Alam<sup>2,b</sup>**  
8 **David C.S. Beddows<sup>2,3</sup>, Dimitrios Bousiotis<sup>2</sup>, Zongbo Shi<sup>2</sup>**  
9 **Leigh R. Crilley<sup>4</sup>, William Bloss<sup>2</sup>, James Brean<sup>2</sup>, Isha Khanna<sup>5,c</sup>**  
10 **and Rulan Verma<sup>6,c</sup>**

11  
12 **<sup>1</sup> Istanbul University-Cerrahpaşa, Engineering Faculty, Environmental**  
13 **Engineering Department, Istanbul, [Türkiyey](#)**

14  
15 **<sup>2</sup> School of Geography, Earth and Environmental Sciences**  
16 **University of Birmingham, Birmingham, B15 2TT, UK**

17  
18 **<sup>3</sup> National Centre for Atmospheric Science**  
19 **University of York, Heslington, York, YO10 5DQ, UK**

20  
21 **<sup>4</sup> Department of Chemistry, York University**  
22 **Toronto, Ontario, M3J 1P3, Canada**

23  
24 **<sup>5</sup> Puget Sound Clean Air Agency, Seattle, Washington, USA 98101**

25  
26 **<sup>6</sup> Institute of research on catalysis and the environment of Lyon - IRCELYON**  
27 **Université De Lyon, 69626 Villeurbanne cedex, France**

28  
29 **Corresponding author: E-mail: [r.m.harrison@bham.ac.uk](mailto:r.m.harrison@bham.ac.uk) (Roy M. Harrison)**

30  
31 **<sup>a</sup> Also at: Department of Environmental Sciences / Centre of Excellence in Environmental**  
32 **Studies, King Abdulaziz University, PO Box 80203, Jeddah, 21589, Saudi Arabia**

33  
34 **<sup>b</sup> Now at: School of Biosciences, University of Nottingham, Sutton Bonington**  
35 **Campus, Leicestershire, LE12 5RD**

36  
37 **<sup>c</sup> Previously at: IIT Delhi, Hauz Khas, New Delhi, India 110016**  
38  
39

## 40 ABSTRACT

41 Delhi is one of the world's most polluted cities, with very high concentrations of airborne  
42 particulate matter. However, little is known on the factors controlling the characteristics of [wide](#)  
43 [range](#) particle number size distributions. Here, new measurements are reported from three field  
44 campaigns conducted in winter, pre-monsoon and post-monsoon seasons on the Indian Institute of  
45 Technology campus in the south of the city. Particle number size distributions were measured  
46 simultaneously using a Scanning Mobility Particle Sizer and a Grimm optical particle monitor,  
47 covering 15 nm to >10  $\mu\text{m}$  diameter. The merged, wide-range size distributions were categorised  
48 into five size ranges: nucleation (15-20 nm), Aitken (20-100 nm), accumulation (100 nm-1  $\mu\text{m}$ ),  
49 large fine (1-2.5  $\mu\text{m}$ ) and coarse (2.5-10  $\mu\text{m}$ ) particles. The ultrafine fraction (15-100 nm) accounts  
50 for about 52 % of all particles by number (PN<sub>10</sub>-[total particle number from 15 nm to 10  \$\mu\text{m}\$](#) ), but  
51 just 1 % by PM<sub>10</sub> volume (PV<sub>10</sub>- [total particle volume from 15 nm to 10  \$\mu\text{m}\$](#) ). The measured size  
52 distributions are markedly coarser than most from other parts of the world, but are consistent with  
53 earlier cascade impactor data from Delhi. Our results suggest substantial aerosol processing by  
54 coagulation, condensation and water uptake in the heavily polluted atmosphere, which takes place  
55 mostly at nighttime and in the morning hours. Total number concentrations are highest in winter,  
56 but the mode of the distribution is largest in the post-monsoon (autumn) season. The accumulation  
57 mode particles dominate the particle volume in autumn and winter, while the coarse mode  
58 dominates in summer. Polar plots show a huge variation between both size fractions in the same  
59 season and between seasons for the same size fraction. The diurnal pattern of particle numbers is  
60 strongly reflective of a road traffic influence upon concentrations, especially in autumn and winter,  
61 [although other sources such as cooking and domestic heating may influence the evening peak.](#)  
62 There is a clear influence of diesel traffic at nighttime when it is permitted to enter the city, and also  
63 indications in the size distribution data of a mode <15 nm, probably attributable to CNG/LPG  
64 vehicles. New particle formation appears to be infrequent, and in this dataset is limited to one day

65 in the summer campaign. Our results reveal that the very high emissions of airborne particles in  
66 Delhi, particularly from traffic, determine the variation of particle number size distributions.  
67

## 68 1. INTRODUCTION

69 Air pollution in Delhi has been studied for many years, and the authorities have implemented several  
70 interventions designed to limit the concentrations. The sulphur content of diesel and petrol fuels was  
71 reduced to 50 ppm during 1996-2010, more than 1300 industries were shut down due to hazardous  
72 emissions, commercial vehicles older than 15 years were gradually taken out of the traffic fleet, and  
73 public transport vehicles and auto-rickshaws were converted to compressed natural gas (CNG) fuel  
74 (Narain and Krupnick, 2007). An odd–even vehicle number plate restriction has been applied during  
75 working days (Chowdhury et al., 2017). Although these measures have reduced gaseous pollutants  
76 (SO<sub>2</sub> and CO) and primary particulate matter, in recent years, several studies have reported that the  
77 PM<sub>2.5</sub> concentrations have been constant or slowly increasing in India, especially in the winter and  
78 autumn seasons (Babu et al., 2013; Balakrishnan et al., 2019; Dandona et al. 2017, Kumar et al.,  
79 2017), except in 2020. In 2020, the PM<sub>2.5</sub> level decreased by approximately 40 %, due to Covid-19  
80 measures (Rodríguez-Urrego and Rodríguez-Urrego 2020; Mahato et al., 2020). Although the overall  
81 emission sources in India are dominated by traffic, industry, construction, and local biomass burning,  
82 haze pollution events in Delhi are frequently related to the large-scale open burning of post-harvest  
83 crop residues/wood during the crop burning season in nearby rural regions (Cusworth et al. 2018;  
84 Bikkina et al. 2019; Kanawade et al., 2020). [Furthermore](#), the sources of particles are mostly local  
85 (Hama et al., 2020), meteorological factors play an important role in influencing concentrations [of](#)  
86 [air pollution](#) (Tiwari et al., 2014; Yadav et al., 2016; Guo et al., 2017; Dumka et al. 2019; Kumar et  
87 al. 2020).

88

89 Annual average PM<sub>2.5</sub> levels range between 81 and 190 µg/m<sup>3</sup> in Delhi and are clearly higher than  
90 the WHO guideline value (5 µg/m<sup>3</sup>) and Indian national limit value (40 µg/m<sup>3</sup>) (Hama et al., 2020).  
91 To the best of our knowledge, most studies in India have focussed on the source apportionment from  
92 chemical profiles of particles (Pant and Harrison, 2012; Jain et al. 2020; Bhandari et al., 2020; Rai  
93 et al., 2020). Mostly they have reported that biomass burning contributes greatly to PM<sub>2.5</sub> [mass](#) while

94 traffic contributes heavily to PM<sub>10</sub> [mass](#) in Delhi. Residential energy use contributes 50 % of the  
95 PM<sub>2.5</sub> [mass](#) concentration and the construction sectors are also ~~evaluated as~~[considered](#) an important  
96 source of particles [mass](#) (Guttikunda et al., 2014; Butt et al., 2016; Conibear et al., 2018).  
97 Furthermore, it is particularly important to understand the absolute contribution and sources of  
98 different sizes of particles within PM<sub>2.5</sub>. A recently published paper by Das et al. (2021) highlighted  
99 that <250 nm particles contribute a significant proportion of the total PM<sub>2.5</sub> [mass](#) and are a potentially  
100 important link with human health.

101

102 The Particle [Number](#) Size Distribution (PNSD) can provide air pollution source apportionment with  
103 high time resolution compared to use of chemical species, and influences the aerosol transport and  
104 transformation profiles in the urban atmosphere and toxicological effects on humans (Wu and Boor,  
105 2021). Many PNSD studies have been conducted in urban, traffic and background sites over the past  
106 decades and three review studies have been published (Vu et al., 2015; Azimi et al., 2014; Wu and  
107 Boor, 2021). There are some studies evaluating the number or mass [particle size distribution \(PSD\)](#)  
108 in Delhi (Mönkkönen et al., 2005; Chelani et al., 2010; Gupta et al., 2011; Pant et al., 2016; Gani et  
109 al., 2020). Harrison (2020) compared PNSDs from Delhi, Beijing and London and reported that the  
110 particles from Delhi are far greater in number with a much larger modal diameter, close to 100 nm.  
111 In a recent paper, Gani et al. (2020) has investigated the PNSD up to 0.5 µm sizes from 2017 to 2018  
112 and reported that rapid coagulation is an important process in Delhi.

113

114 The wide range PNSD is important to describe all sources of inhalable particles (<10 µm). It is not  
115 easy to separately [identify](#) particles arising from resuspension, sea salt and construction, or from brake  
116 wear and combustion or vehicle exhaust, using only [the](#) <0.5 µm particle sizes [range](#). Harrison et al.  
117 2011 reported that using wide range particle sizes in source apportionment ~~is~~[was](#) extremely  
118 successful in identifying the separate contributions of on-road emission including brake wear and  
119 resuspension. Although there are a few studies of wide range particle characterization in Beijing (Jing

120 et al., 2014) and source apportionment in Venice, Italy (Masiol et al., 2016), there has been no  
121 [previous](#) wide range PNSD study in Delhi. In this study, we aimed to interpret particulate matter size  
122 distributions over a wide range (15 nm to 10  $\mu\text{m}$ ) in the winter, post-monsoon and pre-monsoon  
123 seasons in Delhi. Future studies will look at two-step receptor modelling of wide range particulate  
124 matter size distributions and chemical composition in Delhi.

125

## 126 2. METHODS

### 127 2.1 Study Area

128 The measurements were part of the NERC/MoES Air Pollution and Human Health in an Indian mega-  
129 city (APHH-Delhi, [www.urbanair-india.org](http://www.urbanair-india.org)) study, a joint UK-India project addressing air pollution  
130 in Delhi. The sampling location was ~15 m above ground level on the 54<sup>th</sup> floor of the Civil  
131 Engineering Department at the Indian Institute of Technology Delhi (IIT Delhi) campus, located in  
132 New Delhi, representative of an urban background environment (28.545 N, 77.193 E) (Figure S1).  
133 [The measurement station is at a 120 m distance from a major arterial road.](#) As part of APHH-Delhi,  
134 there were three field campaigns: (i) Jan-Feb 2018 (winter), (ii) May-June 2018 (summer; pre-  
135 monsoon) and (iii) Oct-Nov 2018 (autumn; post-monsoon). In all field campaigns, a suite of gas and  
136 particulate phase instrumentation was deployed within a temperature controlled laboratory.

137

138 These sampling periods were representative of conditions for PM and gases during these seasons in  
139 Delhi. We found the average PM<sub>2.5</sub> concentration to be approximately 180  $\mu\text{g}/\text{m}^3$ , 220  $\mu\text{g}/\text{m}^3$  and 120  
140  $\mu\text{g}/\text{m}^3$  for winter, autumn (excluding Diwali) and summer, respectively measured by a TEOM-FDMS  
141 [\(TEOM-Filter Dynamic Measurement System\)](#). Hama et al. (2020) studied the long term (from 2014  
142 to 2017) trends of air pollution in Delhi at 6 stations (residential, commercial, and industrial sites)  
143 and reported that the mean PM<sub>2.5</sub> concentrations ranged between 147 – 248  $\mu\text{g}/\text{m}^3$ , 147 – 248  $\mu\text{g}/\text{m}^3$   
144 and 76 – 135  $\mu\text{g}/\text{m}^3$  for winter, autumn and summer, respectively, and a good correlation between

145 sites within Delhi. This gives reassurance that the PM<sub>2.5</sub> concentrations measured at our site are within  
146 the typical range of those observed in Delhi.

147

## 148 **2.2 Measurements**

149 ~~To measure the particle size range used in this study, two particle instruments were used to collect~~  
150 ~~number size distributions (NSD). For the range 15-640nm, a TSI Scanning Mobility Particle Sizer~~  
151 ~~(SMPS) 3936 was used, consisting of a TSI 3080 Electrostatic Classifier, TSI 3081 DMA and TSI~~  
152 ~~3775 CPC. To extend this range into the coarse mode a GRIMM 1.108 Portable Laser Aerosol~~  
153 ~~Spectrometer and Dust Monitor (GRIMM 1.108) were used alongside the SMPS.~~

154

155 Aerosol particle sizes in the atmosphere span a very wide range from a few nanometers at the lower  
156 end to some tens of micrometers at the upper end. Because of this very wide range of sizes, particle  
157 properties vary considerably across the size spectrum with the behaviour of the smaller particles being  
158 determined by their high mobility and hence diffusivity, whilst at the coarse end of the size  
159 distribution inertial properties are especially important. Due to this divergence in behaviour, no  
160 instrument is capable of measurement of the whole range of particle sizes. ~~The smaller particles are~~  
161 ~~mostly measured as a function of their electric mobility when charged, while the larger particles are~~  
162 ~~counted using their inertial or optical properties. In this study an SMPS (Scanning mobility particle~~  
163 ~~sizer) based on mobility diameters and a GRIMM optical spectrometer were used to count smaller~~  
164 ~~and larger particles, respectively.~~

165 ~~To measure the particle size range used in this study, two particle instruments were used to collect~~  
166 ~~number size distributions (NSD). For the range 15-640nm, a TSI Scanning Mobility Particle Sizer~~  
167 ~~(SMPS) 3936 was used, consisting of a TSI 3080 Electrostatic Classifier, TSI 3081 DMA and TSI~~  
168 ~~3775 CPC. To extend this range into the coarse mode a Portable Laser Aerosol Spectrometer and~~  
169 ~~Dust Monitor (GRIMM 1.108) were used alongside the SMPS.~~

170

171

## 172 2.3 Merging Process

173 Merging procedures have usually been reported for merging SMPS and APS (Aerosol Particle Sizer)  
174 data, but here [Grimm optical spectrometer \(OP\) RIMM](#) data is merged with SMPS data. For a  
175 complete particle size distribution, [simultaneously collected](#), paired hourly averaged particle number  
176 size distributions collected from the SMPS and [GRIMMrimm](#) were merged. The merging procedure  
177 is based on the principle of converting the diameters of the [GrimmRIMM](#)-derived data to a diameter  
178 matching the SMPS-derived data, in the region where the size distribution measurements overlap.  
179 The [GrimmRIMM](#) measures the optical diameter  $d_b^t$  whereas the SMPS measures the mobility  
180 diameter  $d_a^t$  of the particles. Comprehensive descriptions of the procedure and mathematics are given  
181 by DeCarlo et al. (2004) and Schmid et al. (2007). The [GrimmRIMM](#) NSD are translated onto the  
182 extended electrical mobility diameter axis of the SMPS using equation (R1) (Beddows et al. 2010; Liu  
183 et al., 2016; Ondracek et al., 2009).

184

$$185 \quad d_b^t = \frac{d_a^t}{X} \sqrt{\frac{C(d_a^t)}{C(d_b^t)}} \quad (\text{R1})$$

186

187 The Cunningham slip correction factor is given by  $C$  and the unknown variables such as the shape  
188 factor of the particles are accounted for by a free parameter  $X$  (given by equation R2) which is adjusted  
189 until the tails of the SMPS and [GrimmRIMM](#) NSD overlap each other giving a continuous NSD  
190 across the particle size bins measured by the two instruments.

191

$$192 \quad X = \sqrt{\frac{\rho_e^t}{\rho_o}} \quad (\text{R2})$$

193

194 The estimated transition-regime effective density  $\rho_e^t$  (normalised by the unit density,  $\rho_o$ ) typically  
195 ranges from 0.77 to 2.56 g/cm<sup>3</sup> when aerodynamic diameter is used in merging. Detailed



196 information upon the effective particle density based on the geographical regions is seen in the Wu  
197 and Boor (2021) study.

198

199 The merging algorithm (originally programmed in CRAN R) was implemented using Excel  
200 spreadsheets and the solver tool minimised the separation between the tails of the overlapping SMPS  
201 and GRIMMrimm. Due to the imperfect nature of the data, each of the merges was allocated a factor  
202 indicating quality based on whether: (i) there is a successful fit; (ii) the scatter of the data across the  
203 overlapping tails; (iii) the fraction of points on the tail falling onto the fitted curve; and (iv) how  
204 smooth the overlap is (Table S1). The size bins overlap (300-700 nm) between Grimm and SMPS.  
205 This process was repeated for the winter, summer and autumn data sets and any results failing the test  
206 were either repeated or the data removed from the analysis. In all, only 8 samples from 1117 failed  
207 to give an acceptable fit in the merge procedure.

208

## 209 **2.4 Data and Quality Management**

210 Data from SMPS and Grimm RIMM were measured with 1-min resolution. ~~In this study, data sets~~  
211 ~~were used by taking their and converted to~~ hourly averages. ~~Simultaneous measurement data from the~~  
212 ~~SMPS and GRIMM were used.~~ The seasons were categorized as winter, autumn and summer. The  
213 measurements were taken in winter from 12 January 16:00 to 11 February 04:00, in autumn from 24  
214 October 16:00 to 11 November 10:00, in summer 16 May 19:00 to 05 June 15:00 in 2018. There  
215 were 709, 403 and 477 total pairs (hours) in the data sets in winter, autumn and summer, respectively.  
216 But 172, 43 and 257 pairs in winter, autumn and summer, respectively were excluded because of the  
217 non-availability of data at that time. Data coverage is 76 % for winter, 95 % for autumn and 46 % for  
218 summer. Figure S2 in the Supplementary shows hourly mean values of total particle counts for three  
219 seasons. In order to evaluate day and night time PNC (particle number concentration) differences, the  
220 day and night were defined as 07:00-19:00 and 19:00 – 07:00, respectively. All times reported are  
221 local times recorded in Indian Standard Time (IST; GMT+05:30).

222

223 R version 3.1.2 was used to analyse the data (R Core Team, 2015). Firstly, all data were checked for  
224 clean-up of the robustness of the data sets, to detect anomalous records and take out the extreme  
225 values. Data greater than the 99.5<sup>th</sup> percentile were deleted. Diwali time in 2018 (7th of November  
226 2018 from 16:00 to 23:00) was taken out the date set in order to exclude its extreme effect on P<sub>NSD</sub>  
227 values. Particle number concentrations during Diwali time are given in the Supplementary, Figure  
228 S3. There were some single gaps in the data matrixes. These missing data were replaced by linearly  
229 interpolated values from the nearest bins to those samples.

230

231 In the literature, PNCs measured below 1 µm are frequently split into three ranges: nucleation, Aitken  
232 and accumulation (Gani et al., 2020). ~~Size range of modes can be highly variable according to the~~  
233 ~~description of the nucleation size range and maximum measured size.~~ Nucleation size ranges have  
234 variously been described as below 30 nm (Masiol et al. 2016) or below 25 nm (Gani et al., 2020) or  
235 below 20 nm (Wu and Boor, 2021). ~~Despite this, there are also limited studies on wide range P<sub>NSD</sub>,~~  
236 ~~some evaluating~~ Some studies have evaluated wide range P<sub>NSD</sub>s split into 4 ranges (nucleation,  
237 Aitken, accumulation and coarse) (Masiol et al. 2016; Harrison et al., 2011). In this study, the modes  
238 have been aggregated into five size groups: nucleation (15-20 nm), Aitken (20 -100 nm),  
239 accumulation (100 nm – 1 µm), large fine (1 µm – 2.5 µm) and coarse (2.5 µm – 10 µm) based on  
240 merged ~~data using SMPS and GRIMM observations~~. Ultrafine particles (UFP) are considered to be  
241 total PN counts of Nucleation and Aitken modes (<100 nm).

242

243 The particle mass was calculated for the SMPS+OP Grimm merged data, assuming a density of 1.6  
244 g cm<sup>-3</sup> (Gani et al., 2020). Estimation of particle density as a function of size is extremely difficult,  
245 and there are few data for particle density from Delhi. Since Gani et al (2020) used the density of  
246 PM at the same location as in our study, we used the same density value to convert PN to PM mass.

247 Figure S4 shows the comparison of PM<sub>2.5</sub> measured by SMPS+OPGRIMM and TEOM-FDMS in

248 Delhi for the three seasons. Figure S5 shows the comparison of PM<sub>2.5</sub> with relative humidity measured  
249 by SMPS+GRIMM-OP and TEOM in Delhi for the three seasons. A good correlation of the estimated  
250 particle mass with independent measurements with a co-located TEOM-FDMS was observed, except  
251 in summer.

252 The cumulative frequency of observations as a function of particle size was calculated for each hour  
253 of the day. Standard central measures from the cumulative frequency plots were represented by the  
254 geometric mean diameter (GMD) for each size distribution. They were used to examine particle  
255 growth processes. Firstly, the growth of GMD was estimated visually from the diurnal GMD data  
256 plot (Fig. 8). The minimum growth time used for estimation of the growth rate (GR) was selected as  
257 three hours, and if the growth lasted for long enough, the GR was estimated. The observed growth of  
258 the GMD of the particle was quantified by fitting the GMD of particles during the growth process  
259 event over a period of time ‘t’ (eq.1). Detailed information on the method can be found in Sarangi et  
260 al. (2015; 2018).

$$261 \text{Growth rates (nm/hour)-GR} = \frac{d\text{GMD}}{dt} \quad (1)$$

262  
263

### 265 3. RESULTS

#### 266 3.1 Particle Number and Size

267 Table S2 gives the descriptive statistics of particle number counts (#/cm<sup>3</sup>) calculated using every 1-  
268 hour measurements for the nucleation, Aitken, accumulation, large fine and coarse modes between  
269 15 nm and 10 μm in all seasons. Time series of total particle number counts are presented in Figure  
270 S2. The average total PN levels were 36.73x10<sup>3</sup> cm<sup>-3</sup> ~~36,730 #/cm<sup>3</sup>~~ in winter, 29.35x10<sup>3</sup> cm<sup>-3</sup> ~~29,355~~  
271 ~~#/cm<sup>3</sup>~~ in autumn and 18.91x10<sup>3</sup> cm<sup>-3</sup> ~~18,906 #/cm<sup>3</sup>~~ in summer. Generally, the wintertime PN levels  
272 were higher than the other seasons. The wintertime PN levels of nucleation, Aitken and accumulation  
273 modes were ~1.5, 1.8 and 2.2 times higher than in summer, respectively. Similar ratios were obtained  
274 by Guttikunda and Gurjar (2012) in Delhi for particulate matter concentrations. This is attributed to

275 the unfavorable dispersion conditions, including low wind speed and low mixing height during the  
276 winter season. The autumn PN levels of nucleation, Aitken and accumulation modes were ~1.5, 1.3  
277 and 1.9 times higher than in summer, respectively. The wintertime and autumn average PN levels are  
278 similar except for the Aitken mode for which winter is 1.4 times higher than in autumn. However, for  
279 the large fine and coarse modes the PN level was not markedly different between winter, autumn, and  
280 summer. Gani et al. (2020) reported that the average PN levels were  $52.50 \times 10^3 \text{ cm}^{-3}$  ~~52,500 #/cm<sup>3</sup>~~ in  
281 winter,  $43.40 \times 10^3 \text{ cm}^{-3}$  ~~43,400~~ in summer, and  $38.00 \times 10^3 \text{ cm}^{-3}$  ~~38,000 #/cm<sup>3</sup>~~ in autumn in Delhi  
282 measured in 2017. The differences in the magnitude of number counts between the two studies are  
283 potentially explained by the difference in the sampling ~~period~~ ~~time~~ and changes in emissions.

284  
285 Figure 1 shows a comparison of average particle number and volume and the contribution to total  
286 PN. The average PV (particle volume) levels indicate that PV of the Aitken mode is highest in winter,  
287 while the accumulation mode is highest in autumn and the coarse mode is highest in summer. The  
288 contribution of UFP (~~<100nm~~) to numbers is highest in summer (57 %) but their contribution to  
289 volume is the lowest in autumn and summer (<1 %). The contribution to both number and volume  
290 of the accumulation mode is highest in autumn with 51 % and 75 %, respectively. UFP contributions  
291 to total PV are below 1 % in Delhi. Furthermore, it can be seen clearly that the coarse fraction of  
292 particles dominates in summer, while the accumulation mode dominates in autumn and winter.

293 Wu and Boor (2021) analysed the PNSD observations made between 1998 and 2017 in 114 cities in  
294 43 countries around the globe. They reported that there are significant variations in the magnitude of  
295 urban aerosol PNSD among different geographical regions. The main finding of their study is that the  
296 ~~number~~ PNSD in Europe, North America, Australia, and New Zealand are dominated by nucleation-  
297 and Aitken-mode particles while in Central, South, Southeast and East Asia they are dominated by  
298 the substantial contribution from the accumulation mode, which is consistent with our finding. Pant  
299 et al. (2016) report mass size distributions for particulate matter sampled by cascade impactor in Delhi  
300 in winter. The dominant modes appear at around 3-4  $\mu\text{m}$  and 0.6  $\mu\text{m}$ , with a lesser peak at 0.2  $\mu\text{m}$

301 aerodynamic diameter. These are respectively in the coarse (former mode) and accumulation (latter  
302 two modes) ranges as classified in the current study. The largest component of mass was in the  
303 accumulation mode, and the distribution fits well with the pattern of data seen in Figure 1. Major  
304 components of the coarse fraction were Al, Si, Ca and Fe (Pant et al., 2016), suggestive of soil and  
305 street dust as major contributors. The elements most notably in the accumulation fraction were Cu,  
306 Zn, Pb and Sb, indicative of non-exhaust traffic emissions and metallurgical sources, and S, which  
307 showed a major peak due to sulphate, peaking at 0.9  $\mu\text{m}$  (Pant et al., 2016).

308

309

### 310 **3.2 Diurnal Change**

311 Figure 2 shows the diurnal variation of particle number concentrations and of  $\text{PM}_{2.5}$ , BC, NO and  
312  $\text{NO}_2$  for each season (excluding the day of Diwali), and the normalized time variations of all particle  
313 fractions are given in Figure S6. Figure S7 represents the diurnal variation of meteorological  
314 parameters. In general, there are large differences of PN levels between cold seasons (winter and  
315 autumn) and warm season (summer) for nucleation size particles. Coarse mode particle numbers in  
316 the summer are higher than in winter and autumn, except in the evening time. For autumn and winter,  
317 particle counts are similar from 7 am to 7 pm (daytime). However, from 7 pm to 7 am particle counts  
318 in winter are higher than in autumn. The lowest levels for all modes were present during the afternoon  
319 in all seasons (2-4 pm), followed by highest levels during the night in winter (after 8 pm). The winter  
320 and autumn diurnal profiles had two peaks for below 1  $\mu\text{m}$  particle size in the morning and evening  
321 corresponding to the traffic rush hours. But in the summer the same peaks for nucleation, Aitken and  
322 accumulation modes are seen although of smaller magnitude, and one hour earlier comparing to the  
323 winter and autumn. Pant et al. (2016) reported the diurnal variation of traffic at one of the major  
324 arterial roads in Delhi and Dhyani et al. (2019) reported on traffic-related emission. Figure S98 shows  
325 the diurnal variation in traffic at a major road intersection in Delhi. Cars, two/three wheelers, bus and  
326 LCV (light commercial vehicle) fleet numbers increase in the morning, persist throughout daytime  
327 and start to decrease at 22:00. Due to the prohibition of access for heavy-duty diesel vehicles to central

328 Delhi from 6:00 am until 11:00 pm in the night, during the daytime including the traffic rush hours  
329 the HCV (heavy commercial vehicles) number is at its lowest level (Figure S98 or Dhyani et al. 2019).  
330 While road traffic clearly influences the diurnal pattern in PN, other sources including cooking and  
331 domestic combustion are likely to contribute. Small midday PN peaks were observed during the  
332 summer in the nucleation, Aitken and coarse modes. Another study conducted in Delhi reported the  
333 same midday peaks in the warm season and the highest levels in the cold season (Gani et al. 2020),  
334 which may be related to bus and LCV emissions at midday.

335

336 Figure 3 shows the differences in diurnal variations of total PN levels between the weekday and  
337 weekend. These are based upon a small dataset, and hence the rather small differences within a season  
338 may not be meaningful. In winter the PN levels on Saturday and Sunday are higher than on the  
339 weekdays during the night (from 8 pm to 10 am the next day). However, after the morning rush hour  
340 peaks, during the daytime the PN levels are the same for all days. The diurnal variation of PN in the  
341 autumn shows no significant differences among the days with the same main peaks in the morning  
342 for all days, although highest on Saturday. There is a flattened peak (from 8 to 10 am) in the morning  
343 rush hour for the weekday while there are pointed peaks at approximately 9 am on Saturday and  
344 Sunday in winter and autumn. Measurements made during the summer period are very limited. Due  
345 to there being only 4 full days and 9 half days of measurements, it is very hard to draw any  
346 conclusions. Even so, there are indications of a weekday traffic effect upon the PN levels in summer.  
347 There is only one day of measurements on a Sunday (3<sup>rd</sup> June 2018) and it shows the midday peaks.  
348 Overall, despite seasonal differences, there appears to be a strong influence of light duty road vehicles  
349 upon the diurnal profiles, reflecting traffic volumes, with an impact of heavy duty vehicles upon  
350 nighttime concentrations of all particle fractions.

351

352 NPF events present variable seasonality for different areas, though in most cases they appear to be  
353 more frequent during spring or summer (Salvador et al., 2021). Gani et al. 2020 studied long term

354 PNSD in Delhi and have stated that they did not see any NPF during the winter or autumn seasons in  
355 Delhi. In this study, the identification of NPF events was conducted manually using the criteria set  
356 by Dal Maso et al. (2005) and used by Bousiotis et al (2019; 2021). The data were analysed visually  
357 on a day-to-day basis: each 24-hour period, from midnight to midnight. According to these criteria, a  
358 NPF event is considered when: a distinctly new mode of particles appears in the nucleation mode size  
359 range, prevails for some hours, and shows signs of growth. These are the initial criteria used in  
360 identifying the events. Following that, as the dataset starts from a rather large size (15 nm), to be  
361 more confident about the events and not to confuse them with pollution events, high time resolution  
362 data for NO<sub>x</sub> as well as the fluctuations of the condensation sink were also used to identify pollution  
363 events affecting particle concentrations which were not considered. Hence, while we checked the  
364 particle size distributions for the NPF events, we also looked at the levels of pollutants to ensure that  
365 what was attributed to a NPF event was not particles from pollution / direct emissions. By considering  
366 the pollution levels and condensation sink we can reduce the possibility of including particle  
367 formation events that are not associated with secondary formation. After analysing all data,  
368 measurements from only one day during the measurement campaign were compliant with the criteria  
369 set as a class Ia NPF event. Figure 4 presents the contour plots of average diurnal variation for all  
370 seasons and for the NPF event on 3rd June. NPF may be suppressed due to very high pre-existing  
371 aerosol concentrations (Kanawade et al., 2020; Gani et al. 2020) during severe air pollution episodes  
372 in Delhi. This suppression effect has also been observed in European cities (Bousiotis et al., 2019;  
373 2021).

374 [A new study by Sebastian et al. \(2021\) analysed PNSD and the frequency of NPF at six different](#)  
375 [locations in India. The Delhi observation site is in an urban area and located at CSIR-National](#)  
376 [Physical Laboratory \(NPL\), approximately 8 km far from the IIT location described as urban](#)  
377 [background in our study. They found that the NPF frequently occurs in the spring season, but their](#)  
378 [least common in autumn and winter due to air pollution episodes suppressing the NPF. They also](#)  
379 [stated that the highest concentration and frequency of occurrence of NPF events in was Delhi as](#)

380 [compared to other sites. As in other studies \(such as Bousiotis et al., 2021\), this study also emphasized](#)  
381 [that the increased concentrations of precursor gases are more-important for the occurrence of NPF](#)  
382 [and in urban areas.](#)

383

### 384 **3.3 Day and Night Time Differences in PN and PV**

385 Table S3 presents the summary statistics of the particle number and mass levels derived from merged  
386 particle number data and BC, NO<sub>x</sub> and PM<sub>2.5</sub> at night and day for each season, excluding Diwali.  
387 Figure 5 shows the particle number comparison of all modes at night and day seasonally. In both  
388 night and day, the nucleation counts are approximately the same in autumn and summer (N/D=1.1  
389 and 1.0), and a little higher at night in winter (N/D=1.3). But in the night, Aitken and accumulation  
390 counts are higher than in the day by factors of 1.4 and 1.5 times in summer, 1.2 and 1.5 times in  
391 autumn, respectively and approximately 2 in winter. While the coarse mode PN counts are  
392 approximately the same for all seasons and day / night, the large fine PN level in the nighttime are  
393 significantly higher (1.7) than in the daytime in summer. It seems that in the nighttime high PM  
394 concentrations are due to the increasing Aitken and accumulation modes occurring from coagulation  
395 of nucleation mode particles, condensation of low volatility species or hygroscopic growth. In  
396 addition, biomass burning and older diesel vehicles can contribute significantly to particles in these  
397 fractions (Kumar et al., 2013; Chen et al., 2017; Gani et al., 2020). Meteorological factors can also  
398 profoundly affect the PN levels in daytime and nighttime. The differences of wind speed between day  
399 and night in summer are lower than in winter and autumn (Figure S7). Higher wind speed, and lower  
400 humidity, may favour the resuspension of coarse dust as a dominant mechanism in the summer.  
401 Seasonal changes in mixing depths are surprisingly small (Figure S7) and hence unlikely to have a  
402 major influence. [Furthermore However, the major increases and decreases in the diurnal plots of](#)  
403 [pollutants \(Figure 2\) are consistent with the diurnal plots of MLH \(Figure S7\). Autumn and winter](#)  
404 [also have longer periods with low mixing heights, also seen in Figure S7. TPN showed a negative](#)  
405 [exponential dependence upon MLH, which became more scattered at lower values of MLH, probably](#)  
406 [reflecting the larger relative errors in MLH estimates at smaller values.](#)



407 [Figure S8](#) represents the relation between the ventilation coefficients ( $VC = MLH \times \text{wind speed}$ ) and  
408 [TPN](#) as a function of hour and month. [Gani et al. \(2019\)](#) reported that the VC is ~~being~~ 4–6 times  
409 ~~slower~~ smaller for the wintertime compared to the summer in Delhi. In this study, the VC is 1.8 and  
410 1.6 times higher in summer (mean 2732 m<sup>2</sup>/s) compared to the winter (mean 1491 m<sup>2</sup>/s) and autumn  
411 (mean 1702 m<sup>2</sup>/s), respectively. The day-time hourly TPN levels are lower as related to the higher  
412 VC and the lower VC in colder months gives higher TPN. Although there are not enough daily data  
413 (especially for summer) to ~~say~~ give more detail, we can see the same trend as comparing to the weekly  
414 data from [Gani et al \(2019\)](#) study.

415 Overall, for the daytime for all seasons, hourly averaged UFP (~~<100nm~~) concentrations are usually  
416 less than the nighttime, however the UFP contribution to the PN<sub>1</sub> (55 % in day, 50 % in night for  
417 winter; 52 % in day, 45 % in night for autumn; 58 % in day, 56 % in night for summer) and PN<sub>10</sub> (38  
418 % in day, 38 % in night for winter; 40 % in day, 33 % in night for autumn; 36 % in day, 33 % in night  
419 for summer) are mostly slightly higher in the daytime. Similarly, [Gani et al. \(2020\)](#) have reported the  
420 highest contribution (of UFP to PNC) in the daytime compared with the nighttime in Delhi. Due to  
421 the difference of PN size range (they measured down to 12nm), they found the UFP contribution to  
422 PNC higher than in the present study.

423

424

425

### 426 **3.4 Size Distributions**

427 [Figure 65](#) shows the average ~~PNSD~~ particle number size distributions in three seasons in Delhi.  
428 Volume and Area distributions are shown in the Supplementary Materials in [Figure S910](#). The highest  
429 number concentrations are seen in winter, followed by autumn, and then summer. Although the  
430 number concentrations of particles below 200 nm are far greater in winter those between 200 and  
431 600nm are greater in autumn, within the accumulation mode. The winter and summer [PNSD](#) show  
432 modes at approximately 100 nm but the autumn [PNSD](#) shows the mode at approximately 200 nm.  
433 This could be due to changing sources of particles in Delhi between seasons ([Jain et al. 2020](#)), in

434 addition to (differing) aerosol dynamical processes. The Delhi atmosphere is more polluted  
435 comparing with most other cities based on particle number and mass (Harrison, 2020). This will cause  
436 a tendency for particles to grow more rapidly by coagulation and condensation (Harrison et al., 2018),  
437 but this might be expected to occur in all seasons.

438

439 As described above, in Delhi the nighttime particle concentrations are markedly higher than the  
440 daytime concentrations. The PNSD changes for each hour of the day across all three seasons were  
441 analysed (Figure S1149) and categorized. Figure 7 presents the PNSD differences between daytime  
442 and nighttime and shows the variation in PNSDs within the day in all seasons. The main difference  
443 between day and night in winter is only the number concentration, with little change in the mode size  
444 between day and night, while the PNSDs in summer and autumn show bimodal distributions with  
445 modes at approximately 30 and 140 nm in summer, and 35 and 200 nm in autumn. When we focus  
446 on PNSD during the daytime, it can be clearly seen that the modes are manifest at different times: In  
447 winter, while the PNSD shows the same mode at approximately 100 nm from 8 am to 2 pm, the mode  
448 in the afternoon (from 2 pm to 6 pm) drops slightly in size (70 nm). In the morning and afternoon  
449 there are two small peaks at 60 nm and 40 nm for the Aitken fraction and 170 and 130 nm for the  
450 accumulation fraction in autumn. During the day in summer, there are two peaks at approximately 30  
451 nm from 10 am to 6 pm. This may be associated with summer nucleation events and NPF on 3rd June  
452 2018 (Figure 4). Furthermore it may be related to the growth of particles from 10 am to 2 pm in  
453 autumn and summer. The full reasons for these changing PNSDs are not clear, and it would be unwise  
454 to attempt a detailed interpretation of a very small dataset.

455

456 Figure 8 shows the average geometric mean diameter (GMD) change with hour of the day. Two  
457 overall periods of GMD increase are observed. One of them is in nighttime in all seasons with GMD  
458 growing at between 4.6 nm/hour in summer and 6.2 nm/hour in winter. The particle growth in autumn  
459 is predominantly (when compared to the winter and summer) both late in the night (from 0 am to 5

460 am) and in the morning (from 8 am to 12 pm). Considering the [PNSD](#) trend in autumn (Figure 7), the  
461 GMD rises at 9 nm/hour from morning to noon. Similar results were obtained in the USA (Kuang et  
462 al., 2012), Canada (Jeong et al., 2010; Iida et al. 2008), Italy (Hamed et al., 2007) and Japan (Han et  
463 al. 2013). However the calculated GMD growth rate is smaller than that calculated by Sarangi et al.,  
464 (2015; 2018) in Delhi, by Kalafut-Pettibone et al. (2011) in Mexico City and by Zhang et al. (2011)  
465 in Beijing. The changing GMD with time in Delhi could be the result of changing sources, and/or of  
466 dynamics. Nocturnal growth may be the result of reducing temperatures and increasing RH causing  
467 vapour condensation (Sarangi et al., 2018). Morning growth may be due to oxidation processes  
468 leading to production of less volatile vapours which then condense onto the particles (Sarangi et al.  
469 2018).

470

471 Figure 9 gives the average particle number, volume, area and mass size distribution for all seasons.  
472 While the number size distributions have one mode, two peaks are observed in volume distributions,  
473 centered at 0.5  $\mu\text{m}$  and 6  $\mu\text{m}$ . These relate to two different main sources, which might be secondary  
474 aerosol (such as sulphate at high RH) in the fine mode and road dust resuspension, soil or construction  
475 dust for the coarse mode (Pant et al. 2016). In winter and autumn fine mode particle volumes are  
476 higher than the coarse mode. However, in summer the coarse mode particle volumes are higher than  
477 the fine particle level. In a recent paper, Thamban et al. (2021) show that modes in the mass size  
478 distributions of [hydrocarbon organic aerosol \(HOA\)](#), [Semi-volatile oxygenated organic aerosol](#)  
479 [\(SVOOA\)](#), [biomass burning organic aerosol \(BBOA\)](#) and [low-volatile oxygenated organic aerosol](#)  
480 [\(LVOOA\)](#) measured by aerosol mass spectrometry are typically in the range 300-600nm vacuum  
481 aerodynamic diameter, very consistent with the peaks seen in the mass distributions in Figure 9.

482

483 Hama et al. (2020) obtained the spatiotemporal characteristics of daily-averaged air pollutants and  
484 concluded that the particulate matter mass ( $\text{PM}_{10}$  and  $\text{PM}_{2.5}$ ) is dominated by local sources across  
485 Delhi. The main local air pollutant sources in Delhi include traffic, construction, resuspension of dust,

486 diesel generators, power plants, industries and biomass burning (Kumar et al., 2013; Nagpure et al.,  
487 2015; Hama et al., 2020).

488

489 All average PNSD graphs show an increasing trend in PNC at particle sizes below 19 nm particle  
490 diameter. SMPS measurements in this study were conducted only above 15 nm. So, the peak particle  
491 size within this size range cannot be seen. However, the clear increase in particle number below 19  
492 nm indicates that another source may be important in Delhi. This small mode and bimodal PNSD  
493 during the day (Figure 7) may be associated with the road transport vehicle types in Delhi. Despite  
494 the diesel restriction during the rush hours and conversion of the public transport vehicles to CNG,  
495 several studies have reported that PM<sub>2.5</sub> concentrations have been remaining steady or are slowly  
496 increasing in India, especially in the winter and autumn seasons (Babu et al., 2013; Balakrishnan et  
497 al., 2019; Dandona et al. 2017; Kumar et al., 2017).

498

499 The fuels used in Delhi's traffic fleet are petrol, diesel, CNG and LPG. Legislation limits the sulphur  
500 content of the fuel to 50 ppm in diesel as per Bharat Stage IV. The diesel vehicles are not required to  
501 be fitted with particle traps. The technology of the gasoline vehicle fleet varies as vehicle engine  
502 capacity changes. Cars, two/three wheelers, bus and LCV fleet volumes are high during the day. Due  
503 to the time restrictions on trucks/heavy good vehicles entering the city, during the daytime the HCV  
504 number is at its lowest level (Figure S98).

505 Previous published studies indicate that emissions of particles from CNG vehicles (Euro 4, 5, 6) with  
506 diameter greater than 23 nm are as low as a diesel particle filter equipped vehicle, and an order of  
507 magnitude lower than gasoline vehicles (Kontses et al. 2020; Giechaskiel, et al. 2019; Magara-Gomez  
508 et al. 2014; Schreiber et al. 2007), and CNG vehicles mainly emit nuclei-mode particles (Zhu et a.,  
509 2014; Toumasatos et al. (2020). Zhu et al. (2014) calculated size-resolved particle emission factors  
510 from on-road diesel buses and CNG buses and reported that the PNSD of diesel buses dominate the  
511 accumulation mode diameters of 74-87 nm while the PNSD of CNG buses dominated the nucleation

512 mode with modes at 21-24 nm. Total PN emissions of diesel buses per vehicle were 4 times higher  
513 than the level of CNG buses. However, the PN level in the nucleation mode (15-25 nm) of CNG buses  
514 was 1.7 times higher than from the diesel buses in the nucleation mode. Toumasatos et al. (2020)  
515 studied the particle emission performance of the Euro 6 CNG and gasoline vehicles and discussed the  
516 current EU cut-off solid PN size threshold of 23 nm. The results revealed that PN>23 nm represented  
517 43 % of PN>10 nm and 8 % of PN>2.5 nm for gasoline vehicles and 7 % of PN>10 nm and 1 % of  
518 PN>2.5 nm for CNG vehicles respectively. These studies of emission P<sub>N</sub>SDs show that a significant  
519 number of particles reside below the EU lower measurement limit of 23 nm, and many are even  
520 smaller than 10 nm. These probably contribute to the mode seen just appearing at the extreme small  
521 particle limit of Figure 9.

522

523 When the P<sub>N</sub>SD results measured in Delhi are compared with the main emission categories in the  
524 literature (Kumar et al., 2013; Vu et al., 2015), it seems that the average size distributions measured  
525 in the atmosphere in Delhi are much coarser, which is presumably due to condensation and  
526 coagulation, or it could be that secondary particles dominate over the primary emissions. Pant et al.  
527 (2016) hypothesised that the main accumulation mode peak in their winter measurements arose from  
528 aqueous droplet evaporation, although this mechanism would be unlikely to explain the mode seen  
529 in the summer data. Thamban et al. (2021) have also reported particle growth in the Delhi atmosphere  
530 from condensation of organic compounds formed from oxidation processes.

531 Previous studies have attempted to quantify the relative contribution of primary and secondary  
532 sources to the total and mode-segregated particle number concentrations (Kulmala et al. 2021;  
533 Casquero-Vera et al. 2021; Hama et al. 2017; Kulmala et al. 2016; Rodríguez, & Cuevas, 2007).  
534 Rodríguez and Cuevas (2007) first presented the methodology for the separation of traffic related  
535 primary aerosol particles from the total using the BC as the main tracer of traffic. The method was  
536 tested in this study, but did not prove appropriate as the BC sources in Delhi are more complex, and  
537 arise not only from traffic. The BC diurnal trend (Figure 2) does not show the rush hour peaks, and

538 reflects mostly the combustion activity at night, presumably including the heavy duty diesel  
539 emissions. A recent study by Kulmala et al. (2021) used NO<sub>x</sub> as a tracer of primary sources. Figure 2  
540 shows that only the NO<sub>2</sub> diurnal trend in autumn is clearly related to traffic sources. Furthermore the  
541 sources of BC and NO<sub>x</sub> are largely the same, as judged from the high similarity between BC and NO<sub>x</sub>  
542 diurnal trends (Figure 2).

543

### 544 **3.5 Correlations of PN with NO<sub>2</sub>, NO, and BC**

545 Figure 10 shows the correlation coefficients between the hourly average PNs of five particle size  
546 fractions and NO, NO<sub>2</sub>, and BC measured in Delhi. Nucleation mode PN is better correlated with the  
547 Aitken mode PN in winter and summer despite the lower correlation in autumn. The correlations  
548 among >1 μm size fractions are higher in summer than winter and autumn. Tyagi et al. (2016) stated  
549 that the major source of NO<sub>x</sub> emissions is vehicle exhaust and power plants in Delhi. Furthermore,  
550 studies have reported that approximately 80-90 % of NO<sub>x</sub> and CO are produced from the transport  
551 sector in Delhi (Gurjar et al., 2004; Gulia et al., 2015; Tyagi et al., 2016; Hama et al., 2020). As seen  
552 in Figure 2, the NO<sub>2</sub> diurnal trend is very similar to nucleation and Aitken particle trends, especially  
553 in the autumn. NO<sub>2</sub> peaks in autumn in the traffic rush hours are larger than in winter and summer.  
554 In addition, there are no significant correlations between NO<sub>2</sub> and NO or BC in autumn (0.02 for NO,  
555 0.03 for BC) compared to the summer (0.73 for NO, 0.61 for BC) and winter (0.37 for NO and 0.28  
556 for BC) (Figure S12<sup>+</sup>). NO and BC diurnal trends show the same higher level in the night (Figure 2)  
557 and also, they have higher correlation coefficients (0.78 in winter, 0.77 in summer, 0.72 in autumn)  
558 for all seasons, similar to the accumulation mode particle counts (Figure 2, Figure 10, Table S2). NO<sub>2</sub>  
559 and <100 nm particles may be associated with traffic sources, while the NO and BC and <1 μm  
560 particles could be associated with biomass burning, industry, (small generator) power generation, or  
561 possibly also with diesel vehicles.

562

### 563 **3.6 Wind Effects**

564 Figure S1<sup>32</sup> represents polar plots of BC, NO and NO<sub>2</sub> measured in Delhi. This shows no consistent  
565 pattern. There are differences between the pollutants in terms of directional and wind speed  
566 associations, and for each pollutant / season. There is no obvious indication of a strong local source  
567 influence, typically manifest as an intense area in the very centre of the plot circle. The plots for the  
568 particle size fractions (Figure 11) also show little consistency between seasons for a given size  
569 fraction. Within a season, however, adjacent size fractions often show a similarity of behaviour  
570 (consistent with their correlations, see above) but this similarity does not extend across all size ranges  
571 within a season.

572

#### 573 **4. CONCLUSIONS**

574 This study serves to highlight the remarkable complexity of airborne particulate matter in Delhi. The  
575 size distributions show marked seasonal changes, with coarse particles dominant in summer, but not  
576 in the cooler seasons, when the accumulation mode dominates. The measured size distributions show  
577 a fine mode aerosol with a considerably larger modal diameter than that typically seen in western  
578 countries, and larger than the modal emission size from major source categories. It appears that  
579 the high particle concentrations and chemically reactive atmosphere are promoting rapid coagulation  
580 and condensational growth of particles, and therefore the measured size distributions are driven more  
581 by aerosol dynamical processes than source characteristics. Growth via a liquid droplet phase in the  
582 cooler months may also occur. There is little evidence for a contribution of new particle formation  
583 (although the summer season dataset is small), consistent with earlier work by Gani et al. (2020).  
584 Another notable feature is the apparent complexity and seasonal variability of sources of NO, NO<sub>2</sub>  
585 and BC, pollutants which can often be used to identify or locate sources of emissions. This is reflected  
586 in the various particle fractions, which generally correlate poorly with the other pollutants and with  
587 other than proximate size fractions.

588

589 The diurnal variation of all particle fractions is strongly suggestive of a road traffic influence,  
590 especially in the winter campaign. This appears strongly influenced by the emissions of heavy duty  
591 diesel traffic which is only able to access central Delhi at night. A size mode of <15 nm may well  
592 be attributable to vehicles using LPG/CNG fuels. However, the seasonal variability of the geographic  
593 distribution and wind speed dependence of sources revealed by the polar plots is strongly indicative  
594 of many other sources also contributing to all size fractions of particles.

595

#### 596 **DATA ACCESSIBILITY**

597 Data supporting this publication are openly available from the UBIRA eData repository at  
598 <https://doi.org/10.25500/edata.bham.00000730>

599

#### 600 **AUTHOR CONTRIBUTIONS**

601 This study was conceived by RMH. WJB managed the research programme, and MSA and LRC  
602 collected the data. DCB and UAS led the data analysis with contributions from JB and DB. UAS  
603 and RMH co-authored the first draft. ZS and all co-authors provided comments and revisions.

604

#### 605 **COMPETING INTERESTS**

606 The authors declare that they have no conflict of interest.

607

#### 608 **FINANCIAL SUPPORT**

609 This research has been supported by the Natural Environment Research Council NE/P016499/1.

610

#### 611 **ACKNOWLEDGEMENTS**

612 We are thankful the Scientific and Technical Research Council of Turkey (TUBITAK) (grant  
613 number 1059B191801445) to support the author Ulku Alver Sahin to work on the ASAP project.

614 We would also like to acknowledgement the IIT Delhi team under the Principal Investigator-ship of



615 Professor Mukesh Khare who provided all the facilities including space and logistical help during  
616 the experiment.

617

618 **REFERENCES**

619

620 Azimi, P., Zhao, D. and Stephens, B.: Estimates of HVAC filtration efficiency for fine and ultrafine  
621 particles of outdoor origin, *Atmos. Environ.*, 98, 337-346,  
622 <https://doi.org/10.1016/j.atmosenv.2014.09.007>, 2014.

623

624 Babu, S. S., Manoj, M.R., Moorthy, K. K., Mukunda, M. G., Vijayakumar, S.N., Sobhan, K.K.,  
625 Satheesh, S.K., Niranjana, K., Ramagopal, K., Bhuyan, P.K. and Singh, D.: Trends in aerosol optical  
626 depth over Indian region: Potential causes and impact indicators, *J. Geophys. Res.*, 118, 11794–  
627 11806, <https://doi.org/10.1002/2013JD020507>, 2013.

628

629 Balakrishnan, K., Pillarisetti, A., Yamanashita, K. and Yusoff, K.: *Air Pollution in Asia and the*  
630 *Pacific: Science Based Solution*, Published by the United Nations Environment Programme  
631 (UNEP), Chapter 1.2 Air quality and health in Asia and the Pacific, January 2019, ISBN: 978-92-  
632 807-3725-7, Bangkok, Thailand, 2019.

633

634 Beddows, D. C. S., Dall'osto, M. and Harrison, R. M.: An Enhanced Procedure for the Merging of  
635 Atmospheric Particle Size Distribution Data Measured Using Electrical Mobility and Time-of-  
636 Flight Analysers, *Aerosol Science and Technology*, 44, 11, 930-938,  
637 <https://doi.org/10.1080/02786826.2010.502159>, 2010.

638

639 Bhandari, S., Gani, S., Patel, K., Wang, D. S., Soni, P., Arub, Z., Habib, G., Apte, J.S. and Ruiz, L.  
640 H.: Sources and atmospheric dynamics of organic aerosol in New Delhi, India: insights from  
641 receptor modeling, *Atmos. Chem. Phys.*, 20, 735–752, <https://doi.org/10.5194/acp-20-735-2020>,  
642 2020.

643

644 Bikkina, S., Andersson, A., Kirillova, E. N., Holmstrand, H., Tiwari, S., Srivastava, A. K., Bisht,  
645 D.S. and Gustafsson, Ö.: Air quality in megacity Delhi affected by countryside biomass burning,  
646 *Nature Sustainability*, 2, 200–205, <https://doi.org/10.1038/s41893-019-0219-0>, 2019.

647

648 Bousiotis, D., Dall'Osto, M., Beddows, D. C. S., Pope, F. D., and Harrison, R. M.: Analysis of new  
649 particle formation (NPF) events at nearby rural, urban background and urban roadside sites, *Atmos.*  
650 *Chem. Phys.*, 19, 5679–5694, <https://doi.org/10.5194/acp-19-5679-2019>, 2019.

651

652 Bousiotis, D., Brean, J., Pope, F. D., Dall'Osto, M., Querol, X., Alastuey, A., Perez, N., Petäjä, T.,  
653 Massling, A., Nøjgaard, J. K., Nordstrøm, C., Kouvarakis, G., Vratolis, S., Eleftheriadis, K., Niemi,  
654 J. V., Portin, H., Wiedensohler, A., Weinhold, K., Merkel, M., Tuch, T., and Harrison, R. M.: The  
655 effect of meteorological conditions and atmospheric composition in the occurrence and  
656 development of new particle formation (NPF) events in Europe, *Atmos. Chem. Phys.*, 21, 3345–  
657 3370, <https://doi.org/10.5194/acp-21-3345-2021>, 2021.

658

659 Butt, E. W., Rap, A., Schmidt, A., Scott, C. E., Pringle, K. J., Reddington, C. L., Richards, N. A.  
660 D., Woodhouse, M. T., Ramirez-Villegas, J., Yang, H., Vakkari, V., Stone, E. A., Rupakheti, M., S.  
661 Praveen, P., G. van Zyl, P., P. Beukes, J., Josipovic, M., Mitchell, E. J. S., Sallu, S. M., Forster, P.  
662 M., and Spracklen, D. V.: The impact of residential combustion emissions on atmospheric aerosol,  
663 human health, and climate, *Atmos. Chem. Phys.*, 16, 873–905, [https://doi.org/10.5194/acp-16-873-](https://doi.org/10.5194/acp-16-873-2016)  
664 2016, 2016.

665

666 Casquero-Vera, J. A., Lyamani, H., Titos, G., Minguillón, M. C., Dada, L., Alastuey, A., Querol,  
667 X., Petäjä, T., Olmo, F. J. and Alados-Arboledas, L.: Quantifying traffic, biomass burning and  
668 secondary source contributions to atmospheric particle number concentrations at urban and

669 suburban sites, *Science of The Total Environment*, 768, 145282,  
670 [doi.org/10.1016/j.scitotenv.2021.145282](https://doi.org/10.1016/j.scitotenv.2021.145282), 2021.

671

672 Chelani, A. B., Gajghate, D. G., ChalapatiRao, C. V. and Devotta, S.: Particle Size Distribution in  
673 Ambient Air of Delhi and Its Statistical Analysis, *Bull. Environ. Contam. Toxicol.*, 85, 22–27,  
674 <https://doi.org/10.1007/s00128-010-0010-4>, 2010.

675

676 Chen, F., Zhang, X., Zhu, X., Zhang, H., Gao, J. and Hopke, P. K.: Chemical Characteristics of  
677 PM<sub>2.5</sub> during a 2016 Winter Haze Episode in Shijiazhuang, China. *Aerosol Air Qual. Res.*, 17,  
678 368-380, <https://doi.org/10.4209/aaqr.2016.06.0274>, 2017.

679

680 Chowdhury, S., Dey, S., Tripathi, S. N., Beig, G., Mishra, A. K. and Sharma, S.:” Traffic  
681 intervention” policy fails to mitigate air pollution in megacity Delhi, *Environmental Science &*  
682 *Policy*, 74, 8-13, <https://doi.org/10.1016/j.envsci.2017.04.018>, 2017.

683

684 Conibear, L., Butt, E. W., Knote, C., Arnold, S. R. and Spracklen, D. V.: Residential energy use  
685 emissions dominate health impacts from exposure to ambient particulate matter in Indi,. *Nat.*  
686 *Commun.*, 9, 617, <https://doi.org/10.1038/s41467-018-02986-7>, 2018.

687

688 Cusworth, D. H., Mickley, L. J., Sulprizio, M. P., Liu, T., Marlier, M.E., DeFries, R. S.,  
689 Guttikunda, S.K. and Gupta, P.: Quantifying the influence of agricultural fires in northwest India on  
690 urban air pollution in Delhi, India, *Environ. Res. Lett.*, 13, 044018, [https://doi.org/10.1088/1748-](https://doi.org/10.1088/1748-9326/aab303)  
691 [9326/aab303](https://doi.org/10.1088/1748-9326/aab303), 2018.

692

693 Dal Maso, M., Kulmala, M., Riipinen, I., Wagner, R., Hussein, T., Aalto, P. P. and Lehtinen, K. E.  
694 J.: Formation and growth of fresh atmospheric aerosols: eight years of aerosol size distribution data  
695 from SMEAR II, Hyytiälä, Finland, *Boreal Environmental Research* 10, 323-336, 2005.

696

697 Dandona, L., Dandona, R., Kumar, G. A., Shukla, D. K., Paul, V. K., Balakrishnan, K.,  
698 Prabhakaran, D., Tandon, N., Salvi, S., Dash, A. P., Nandakumar, A., Patel, V., Agarwal, S. K.,  
699 Gupta, P. C., Dhaliwal, R. S., Mathur, P., Laxmaiah, A., Dhillon, P. K., Dey, S., Mathur, M. R.,  
700 Afshin, A., Fitzmaurice, C., Gakidou, E., Gething, P., Hay, S.I., Kassebaum, N. J., Kyu, H., Lim, S.  
701 S., Naghavi, M., Roth, G. A., Stanaway, J. D., Whiteford, H., Chadha, V. K., Khaparde, S. D., Rao,  
702 R., Rade, K., Dewan, P., Furtado, M., Dutta, E., Varghese, C. M., Mehrotra, R., Jambulingam, P.,  
703 Kaur, T., Sharma, M., Singh, S., Arora, R., Rasaily, R., Anjana, R. M., Mohan, V., Agrawal, A.,  
704 Chopra, A., Mathew, A. J., Bhardwaj, D., Muraleedharan, P., Mutreja, P., Bienhoff, K., Glenn, S.,  
705 Abdulkader, R. S., Aggarwal, A. N., Aggarwal, R., Albert, S., Ambekar, A., Arora, M., Bachani,  
706 D., Bavdekar, A., Beig, G., Bhansali, A., Bhargava, A., Bhatia, E., Camara, B., Christopher, D. J.,  
707 Das, S. K., Dave, P. V., Dey, S., Ghoshal, A. G., Gopalakrishnan, N., Guleria, R., Gupta, R., Gupta,  
708 S. S., Gupta, T., Gupte, M. D., Gururaj, G., Harikrishnan, S., Iyer, V., Jain, S.K., Jeemon, P.,  
709 Joshua, V., Kant, R., Kar, A., Katakai, A.C., Katoch, K., Khera, A., Kinra, S., Koul, P.A., Krishnan,  
710 A., Kumar, A., Kumar, R. K., Kumar, R., Kurpad, A., Ladusingh, L., Lodha, R., Mahesh, P. A.,  
711 Malhotra, R., Mathai, M., Mavalankar, D., Mohan Bv, M., Mukhopadhyay, S., Murhekar, M.,  
712 Murthy, G.V.S., Nair, S., Nair, S. A., Nanda, L., Nongmaithem, R. S., Oommen, A.M., Pandian,  
713 J.D., Pandya, S., Parameswaran, S., Pati, S., Prasad, K., Prasad, N., Purwar, M., Rahim, A., Raju,  
714 S., Ramji, S., Rangaswamy, T., Rath, G. K., Roy, A., Sabde, Y., Sachdeva, K. S., Sadhu, H., Sagar,  
715 R., Sankar, M. J., Sharma, R., Shet, A., Shirude, S., Shukla, R., Shukla, S. R., Singh, G., Singh, N.  
716 P., Singh, V., Sinha, A., Sinha, D. N., Srivastava, R. K., Srividya, A., Suri, V., Swaminathan, R.,  
717 Sylaja, P. N., Tandale, B., Thakur, J. S., Thankappan, K.R., Thomas, N., Tripathy, S., Varghese,  
718 M., Varughese, S., Venkatesh, S., Venugopal, K., Vijayakumar, L., Xavier, D., Yajnik, C. S.,  
719 Zachariah, G., Zodpey, S., Rao, J. V. R. P., Vos, T., Reddy, K. S., Murray, C. J. L. and  
720 Swaminathan, S.: Nations within a nation: variations in epidemiological transition across the states

721 of India, 1990-2016 in the global burden of disease study. *The Lancet*, 390, 10111, 2437-2460,  
722 [https://doi.org/10.1016/S0140-6736\(17\)32804-0](https://doi.org/10.1016/S0140-6736(17)32804-0), 2017.

723

724 Das, A., Kumar, A., Habib, G. and Vivekanandan, P.: Insights on the biological role of ultrafine  
725 particles of size  $PM_{<0.25}$ : A prospective study from New Delhi, *Environmental Pollution*, 268, Part  
726 B, 115638, <https://doi.org/10.1016/j.envpol.2020.115638>, 2021.

727

728 DeCarlo, P. F., Slowik, J. G., Worsnop, D. R., Davidovits, P. and Jimenez, J. L.: Particle  
729 Morphology and Density Characterization by Combined Mobility and Aerodynamic Diameter  
730 Measurements. Part 1: Theory, *Aerosol Science and Technology*, 38:12, 1185-  
731 1205, <https://doi.org/10.1080/027868290903907>, 2004.

732

733 Dhyani, R., Sharma, N. and Advani, M.: Estimation of Fuel Loss and Spatial-Temporal Dispersion  
734 of Vehicular Pollutants at a Signalized Intersection in Delhi City, India. *WIT Transaction on  
735 Ecology and the Environment: Air Pollution 2019*, WIT Press, 236, 233-247, ISBN: 978-1-78466-  
736 343-8, Editor: Passerini et al., 2019.

737

738 Dumka, U. C., Tiwari, S., Kaskaoutis, D. G., Soni, V. K., Safai, P. D. and Attri, S. D.: Aerosol and  
739 pollutant characteristics in Delhi during a winter research campaign, *Environ. Sci. Pollut. Res.*, 26,  
740 3771–3794. <https://doi.org/10.1007/s11356-018-3885-y>, 2019.

741

742 Gani S., Bhandari, S., Patel, K., Seraj, S., Soni, P., Arub, Z., Habib, G., Ruiz, L.H. and Apte, J.S.:  
743 Particle number concentrations and size distribution in a polluted megacity: the Delhi Aerosol  
744 Supersite study, *Atmos. Chem. Phys.*, 20, 8533–8549, <https://doi.org/10.5194/acp-20-8533-2020>,  
745 2020.

746

747 Giechaskiel, B., Lähde, T. and Drossinos, Y. Regulating particle number measurements from the  
748 tailpipe of light-duty vehicles: The next step?, *Environmental Research*, 172, 1-9,  
749 <https://doi.org/10.1016/j.envres.2019.02.006>, 2019.

750

751 Gulia, S., Shiva Nagendra, S.M., Khare, M. and Khanna, I.: Urban air quality management-A  
752 review, *Atmospheric Pollution Research*, 6, 2, 286-304, <https://doi.org/10.5094/APR.2015.033>,  
753 2015.

754

755 Guo, H., Kota, S.H., Sahu, S.K., Hu, J., Ying, Q., Gao, A. and Zhang, H.: Source apportionment of  
756  $PM_{2.5}$  in North India using source-oriented air quality models, *Environmental Pollution*, 231, 1,  
757 426-436, <https://doi.org/10.1016/j.envpol.2017.08.016>, 2017.

758

759 Gupta, S., Kumar, K., Srivastava, A., Srivastava, A. and Jain, V. K.: Size distribution and source  
760 apportionment of polycyclic aromatic hydrocarbons (PAHs) in aerosol particle samples from the  
761 atmospheric environment of Delhi, India, *Science of The Total Environment*, 409, 22, 4674-4680,  
762 <https://doi.org/10.1016/j.scitotenv.2011.08.008>., 2011.

763

764 Gurjar, B. R., van Aardenne, J. A., Lelieveld, J. and Mohan, M.: Emission estimates and trends  
765 (1990–2000) for megacity Delhi and implications, *Atmospheric Environment*, 38, 33, 5663-5681,  
766 <https://doi.org/10.1016/j.atmosenv.2004.05.057>, 2004.

767

768 Guttikunda, S. K., Goel, R. and Pant, P.: Nature of air pollution, emission sources, and management  
769 in the Indian cities, *Atmospheric Environment*, 95, 501-510,  
770 <https://doi.org/10.1016/j.atmosenv.2014.07.006>, 2014.

771 Guttikunda, S.K. and Gurjar, B.R.: Role of meteorology in seasonality of air pollution in megacity  
772 Delhi, India, *Environ. Monit. Assess.*, 184, 3199–3211. <https://doi.org/10.1007/s10661-011-2182-8>,  
773 2012.  
774  
775 Hama, S.M.L., Kumar, P., Harrison, R.M., Bloss, W.J., Khare, M., Mishra, S., Namdeo, A., Sokhi,  
776 R., Goodman, P. and Sharma, C.: Four-year assessment of ambient particulate matter and trace  
777 gases in the Delhi-NCR region of India, *Sustainable Cities and Society*, 54, 102003,  
778 <https://doi.org/10.1016/j.scs.2019.102003>, 2020.  
779  
780 Hama, S.M.L., Cordell, R. L. and Monks, P. S.: Quantifying primary and secondary source  
781 contributions to ultrafine particles in the UK urban background, *Atmos. Environ.*, 166, 62-78,  
782 [doi.org/10.1016/j.atmosenv.2017.07.013](https://doi.org/10.1016/j.atmosenv.2017.07.013), 2017.  
783  
784 Hamed, A., Joutsensaari, J., Mikkonen, S., Sogacheva, L., Dal Maso, M., Kulmala, M., Cavalli, F.,  
785 Fuzzi, S., Facchini, M. C., Decesari, S., Mircea, M., Lehtinen, K. E. J., and Laaksonen, A.:  
786 Nucleation and growth of new particles in Po Valley, Italy, *Atmos. Chem. Phys.*, 7, 355–376,  
787 <https://doi.org/10.5194/acp-7-355-2007>, 2007.  
788  
789 Han, Y., Iwamoto, Y., Nakayama, T., Kawamura, K., Hussein, T. and Mochida, M.: Observation of  
790 new particle formation over a mid-latitude forest facing the North Pacific, *Atmos. Environ.*, 64, 77-  
791 84, <https://doi.org/10.1016/j.atmosenv.2012.09.036>, 2013.  
792  
793 Harrison RM.: Airborne particulate matter, *Phil. Trans. R. Soc. A*, 378, 20190319.  
794 <http://dx.doi.org/10.1098/rsta.2019.0319>, 2020.  
795  
796 Harrison, R. M., Rob MacKenzie, A., Xu, H., Alam, M. S., Nikolova, I., Zhong, J., ... and Liang, Z.,  
797 Diesel exhaust nanoparticles and their behaviour in the atmosphere. *Proceedings of the Royal*  
798 *Society A*, 474(2220), 20180492, 2018.  
799  
800 Harrison, R. M., Beddows, D.C.S. and Dall'Osto, M.: PMF Analysis of Wide-Range Particle Size  
801 Spectra Collected on a Major Highway, *Environ. Sci. Technol.*, 45, 13, 5522–5528,  
802 <https://doi.org/10.1021/es2006622>, 2011.  
803  
804 Jain, S., Sharma, S. K., Vijayan, N., Mandal, T. K.: Seasonal characteristics of aerosols (PM<sub>2.5</sub> and  
805 PM<sub>10</sub>) and their source apportionment using PMF: A four year study over Delhi, India,  
806 *Environmental Pollution*, 262, 114337, <https://doi.org/10.1016/j.envpol.2020.114337>, 2020.  
807  
808 Jeong, C.H., Evans, G. J., McGuire, M. L., Chang, R. Y.W. and Abbatt, J. P. D.: Zeromskiene, K.,  
809 Mozurkewich, M., Li, S.-M., and Leitch, W. R.: Particle formation and growth at five rural and  
810 urban sites, *Atmos. Chem. Phys.*, 10, 7979–7995, <https://doi.org/10.5194/acp-10-7979-2010>, 2010.  
811  
812 Jing, H., Li, Y.F., Zhao, J., Li, B., Sun, J., Chen, R., Gao, Y. and Chen, C.: Wide-range particle  
813 characterization and elemental concentration in Beijing aerosol during the 2013 Spring Festival,  
814 *Environmental Pollution*, 192, 204-211, <https://doi.org/10.1016/j.envpol.2014.06.003>, 2014.  
815  
816 Kalafut-Pettibone, A. J., Wang, J., Eichinger, W. E., Clarke, A., Vay, S. A., Blake, D. R., and  
817 Stanier, C. O.: Size-resolved aerosol emission factors and new particle formation/growth activity  
818 occurring in Mexico City during the MILAGRO 2006 Campaign, *Atmos. Chem. Phys.*, 11, 8861–  
819 8881, <https://doi.org/10.5194/acp-11-8861-2011>, 2011.  
820

821 Kanawade, V.P., Srivastava, A.K., Ram, K., Asmi, E., Vakkari, V., Soni, V.K., Varaprasad, V. and  
822 Sarangi, C.: What caused severe air pollution episode of November 2016 in New Delhi?, *Atmos.*  
823 *Environ.*, 222, 117125, <https://doi.org/10.1016/j.atmosenv.2019.117125>, 2020.  
824

825 Kontses, A., Triantafyllopoulos, G., Ntziachristos, L. and Samaras, Z.: Particle number (PN)  
826 emissions from gasoline, diesel, LPG, CNG and hybrid-electric light-duty vehicles under real-world  
827 driving conditions, *Atmos. Environ.*, 222, 117126, <https://doi.org/10.1016/j.atmosenv.2019.117126>,  
828 2020.  
829

830 Kuang, C., Chen, M., Zhao, J., Smith, J., McMurry, P. H., and Wang, J.: Size and time-resolved  
831 growth rate measurements of 1 to 5 nm freshly formed atmospheric nuclei, *Atmos. Chem. Phys.*,  
832 12, 3573–3589, <https://doi.org/10.5194/acp-12-3573-2012>, 2012.  
833

834 Kulmala, M., Dada, L., Daellenbach, K.r., Yan, C., Stolzenburg, D., Kontkanen, J., Ezhova, E.,  
835 Hakala, S., Tuovinen, S., Kokkonen, T.V., Kurpp, M., Cai, R., Zhou, Y., Yin, R., Baalbaki, R.,  
836 Chan, T., Chu, B., Deng, C., Fu, Y., Ge, M., He, H., Heikkinen, L., Junninen, H., Liu, Y., Lu, Y.,  
837 Nie, W., Rusanen, A., Vakkari, V., Wang, Y., Yang, G., Yao, L., Zheng, J., Kujansuu, J.,  
838 Kangasluoma, J., Petäjä, T., Paasonen, P., Järvi, L., Worsnop, D., Ding, A., Liu, Y., Wang, L.,  
839 Jiang, J., Bianchi, F. and Kerminen, V.M.: Is reducing new particle formation a plausible solution to  
840 mitigate particulate air pollution in Beijing and other Chinese megacities? *Faraday Discussion* 226,  
841 221, [doi.org/10.1039/D0FD00078G](https://doi.org/10.1039/D0FD00078G), 2021.  
842

843 Kulmala M., Luoma K., Virkkula A., Petäjä T., Paasonen P., Kerminen V.-M., Nie W., Qi X., Shen  
844 Y., Chi X. and Ding A.: On the mode-segregated aerosol particle number concentration load:  
845 contributions of primary and secondary particles in Hyytiälä and Nanjing. *Boreal, Env. Res.*, 21,  
846 319–331. 2016.  
847

848 Kumar, A., Ambade, B., Sankar, T. K., Sethi, S. S. and Kurwadkar, S.: Source identification and  
849 health risk assessment of atmospheric PM<sub>2.5</sub>-bound polycyclic aromatic hydrocarbons in  
850 Jamshedpur, India, *Sustainable Cities and Society*, 52, 101801,  
851 <https://doi.org/10.1016/j.scs.2019.101801>, 2020.  
852

853 Kumar, P., Gulia, S., Harrison, R. M. and Khare, M.: The influence of odd–even car trial on fine  
854 and coarse particles in Delhi, *Environmental Pollution*, 225, 20-30,  
855 <https://doi.org/10.1016/j.envpol.2017.03.017>, 2017.  
856

857 Kumar, P., Pirjola, L., Ketzel, M., and Harrison, R. M.: Nanoparticle emissions from 11 non-  
858 vehicle exhaust sources – A review, *Atmos. Environ.*, 67, 252–277,  
859 <https://doi.org/10.1016/j.atmosenv.2012.11.011>, 2013.  
860

861 Iida, K., Stolzenburg, M.R., McMurry, P.H. and Smith, J.N.: Estimating nanoparticle growth rates  
862 from size-dependent charged fractions: Analysis of new particle formation events in Mexico City,  
863 *J. Geophys. Res.*, 113, D05207, [doi.org/10.1029/2007JD009260](https://doi.org/10.1029/2007JD009260), 2008  
864

865 Liu, J., Jiang, J., Zhang, Q., Deng, J., and Hao, J.: A spectrometer for measuring particle size  
866 distributions in the range of 3 nm to 10 μm, *Front. Environ. Sci. Eng.*, 10, 63–72,  
867 <https://doi.org/10.1007/s11783-014-0754-x>, 2016.  
868

869 Magara-Gomez, K.T., Olson, M.R., McGinnis, J.E., Zhang, M. and Schauer, J.J.: Effect of Ambient  
870 Temperature and Fuel on Particle Number Emissions on Light-Duty Spark-Ignition Vehicles,  
871 *Aerosol Air Qual. Res.*, 14, 1360-1371. <https://doi.org/10.4209/aaqr.2013.06.0183>, 2014.  
872



873 Mahato, S., Pal, S. and Ghosh, K. G.: Effect of lockdown amid COVID-19 pandemic on air quality  
874 of the megacity Delhi, India, *Science of The Total Environment*, 730, 139086,  
875 <https://doi.org/10.1016/j.scitotenv.2020.139086>, 2020.  
876

877 Masiol, M., Vu, T. V., Beddows, D. C. S. and Harrison, R. M.: Source apportionment of wide range  
878 particle size spectra and black carbon collected at the airport of Venice (Italy), *Atmospheric*  
879 *Environment*, 139, 56-74, <https://doi.org/10.1016/j.atmosenv.2016.05.018>, 2016.  
880

881 Mönkkönen, P., Koponen, I. K., Lehtinen, K. E. J., Hämeri, K., Uma, R., and Kulmala, M.:  
882 Measurements in a highly polluted Asian mega city: observations of aerosol number size  
883 distribution, modal parameters and nucleation events, *Atmos. Chem. Phys.*, 5, 57–66,  
884 <https://doi.org/10.5194/acp-5-57-2005>, 2005.  
885

886 Nagpure, A.S., Ramaswami, A. and Russell, A.: Characterizing the Spatial and Temporal Patterns  
887 of Open Burning of Municipal Solid Waste (MSW) in Indian Cities, *Environ. Sci. Technol.*, 49, 21,  
888 12904–12912, <https://doi.org/10.1021/acs.est.5b03243>, 2015.  
889

890 Narain, U. and Krupnick, A., The Impact of Delhi's CNG Program on Air Quality. RFF Discussion  
891 Paper No. 07-06, Available at  
892 SSRN: <https://ssrn.com/abstract=969727> or <http://dx.doi.org/10.2139/ssrn.969727>, 2007.  
893

894 Ondráček, J., Ždímal, V., Smolík, J., and Lazaridis, M.: A Merging Algorithm for Aerosol Size  
895 Distribution from Multiple Instruments, *Water Air Soil Pollut.*, 199, 219–233,  
896 <https://doi.org/10.1007/s11270-008-9873-y>, 2009.  
897

898 Pant, P. and Harrison, R. M.: Critical Review of Receptor Modelling for Particulate Matter: A Case  
899 Study of India, *Atmos. Environ.*, 49, 1-12, <https://doi.org/10.1016/j.atmosenv.2011.11.060>, 2012.  
900

901 Pant, P., Baker, S. J., Goel, R., Guttikunda, S., Goel, A., Shukla, A. and Harrison, R.M.: Analysis of  
902 size-segregated winter season aerosol data from New Delhi, India, *Atmos. Poll. Res.*, 7, 1, 100-109,  
903 <https://doi.org/10.1016/j.apr.2015.08.001>, 2016.  
904

905 R Core Team, 2015. R: a Language and Environment for Statistical Computing. R Foundation for  
906 Statistical Computing, Vienna, Austria. <http://www.R-project.org/>.  
907

908 Rai, P., Furger, M., Haddad, I.E., Kumar, V., Wang, L., Singh, A., Dixit, K., Bhattu, D., Petit, J.E.,  
909 Ganguly, D., Rastogi, N., Baltensperger, U., Tripathi, S.N., Slowik, J.G. and Prévôt, A.S.H.: Real-  
910 time measurement and source apportionment of elements in Delhi's atmosphere, *Science of The*  
911 *Total Environment*, 742, 140332, <https://doi.org/10.1016/j.scitotenv.2020.140332>, 2020.  
912

913 Rodríguez, S. and Cuevas, E.: The contributions of “minimum primary emissions” and “new  
914 particle formation enhancements” to the particle number concentration in urban air, *Journal of*  
915 *Aerosol Science* 38, 1207-1219, <https://doi.org/10.1016/j.jaerosci.2007.09.001>, 2007.  
916

917 Rodríguez-Urrego, D. and Rodríguez-Urrego, L.: Air quality during the COVID-19: PM2.5 analysis  
918 in the 50 most polluted capital cities in the world, *Environmental Pollution*, 266, 1, 115042,  
919 <https://doi.org/10.1016/j.envpol.2020.115042>, 2020.  
920

921 Salvador, P., Barreiro, M., Gómez-Moreno, F. J., Alonso-Blanco, E. and Artúñano, B.: Synoptic  
922 classification of meteorological patterns and their impact on air pollution episodes and new particle  
923 formation processes in a south European air basin, *Atmos.c Environ.*, 245, 118016,  
924 <https://doi.org/10.1016/j.atmosenv.2020.118016>, 2021.

925 Sarangi, B., Aggarwal, S. G., and Gupta, P. K.: A simplified approach to calculate particle growth  
926 rate due to self-coagulation, scavenging and condensation using SMPS measurements during a  
927 particle growth event in New Delhi, *Aerosol and air quality research*, 15(1), 166-179, [https://doi:  
928 10.4209/aaqr.2013.12.0350](https://doi.org/10.4209/aaqr.2013.12.0350), 2015.  
929

930 Sarangi, B., Aggarwal, S. G., Kunwar, B., Kumar, S., Kaur, R., Sinha, D., Tiwari, S. and  
931 Kawamura, K.: Nighttime particle growth observed during spring in New Delhi: Evidences for the  
932 aqueous phase oxidation of SO<sub>2</sub>, *Atmospheric environment*, 188, 82-96,  
933 <https://doi.org/10.1016/j.atmosenv.2018.06.018>, 2018  
934

935 Schmid, O., Karg, E., Hagen, D. E., Whitefield, P. D. and Ferron, G. A.: On the Effective Density  
936 of Non-Spherical Particles as Derived From Combined Measurements of Aerodynamic and  
937 Mobility Equivalent Size, *Atmos. Environ.*, 38, 431–443.  
938 <https://doi.org/10.1016/j.jaerosci.2007.01.002>, 2007.  
939

940 Schreiber, D., Forss, A. M., Mohr, M. and Dimopoulos, P.: Particle Characterisation of Modern  
941 CNG, Gasoline and Diesel Passenger Cars, 8th International Conference on Engines for  
942 Automobiles, Technical Paper 2007-24-0123, ISSN: 0148-7191, e-ISSN: 2688-3627,  
943 <https://doi.org/10.4271/2007-24-0123>, 2007.  
944

945 Tiwari, S., Bisht, D.S., Srivastava, A.K., Pipal, A.S., Taneja, A., Srivastava, M.K. and Attri, S.D.:  
946 Variability in atmospheric particulates and meteorological effects on their mass concentrations over  
947 Delhi, India, *Atmospheric Research*, 145–146, 45-56,  
948 <https://doi.org/10.1016/j.atmosres.2014.03.027>, 2014.  
949

950 [Thamban, N.M., Lalchandani, V., Kumar, V., Mishra, S., Bhattu, D., Slowik, J.G., Prevot, A.S.H.,  
951 Satish, R., Rastogi, N., Tripathi, S.N.: Evolution of size and composition of fine particulate matter  
952 in the Delhi megacity during later winter, \*Atmospheric Environment\*, 267,118752,  
953 \[doi.org/10.1016/j.atmosenv.2021.118752\]\(https://doi.org/10.1016/j.atmosenv.2021.118752\). 2021.  
954](https://doi.org/10.1016/j.atmosenv.2021.118752)

955 Toumasatos, Z., Kontses, A., Doulgeris, S., Samaras, Z. and Ntziachristos, L.: Particle emissions  
956 measurements on CNG vehicles focusing on Sub-23nm, *Aerosol Science and Technology*, 55,  
957 2, 182-193, <https://doi.org/10.1080/02786826.2020.1830942>, 2021.  
958

959 Tyagi, S., Tiwari, S., Mishra, A., Hopke, P.K., Attri, S.D., Srivastava, A.K. and Bisht, D. S.: Spatial  
960 variability of concentrations of gaseous pollutants across the National Capital Region of Delhi,  
961 India, *Atmospheric Pollution Research*, 7, 5, 808-816, <https://doi.org/10.1016/j.apr.2016.04.008>,  
962 2016.  
963

964 Vu, T. V., Delgado-Saborit, J. M. and Harrison, R. M.: Particle number size distributions from  
965 seven major sources and implications for source apportionment studies. *Atmospheric Environment*,  
966 122, 114-132, <https://doi.org/10.1016/j.atmosenv.2015.09.027>, 2015.  
967

968 Wu, T. and Boor, B. E.: Urban aerosol size distributions: a global perspective, *Atmos. Chem. Phys.*,  
969 21, 8883–8914, <https://doi.org/10.5194/acp-21-8883-2021>, 2021.  
970

971 Yadav, R., Sahu, L.K., Beig, G. and Jaaffrey, S.N.A.: Role of long-range transport and local  
972 meteorology in seasonal variation of surface ozone and its precursors at an urban site in India,  
973 *Atmospheric Research*, 176–177, 96-107, <https://doi.org/10.1016/j.atmosres.2016.02.018>, 2016.  
974

975 Zhang, Y. M., Zhang, X. Y., Sun, J. Y., Lin, W. L., Gong, S. L., Shen, X. J. and Yang, S.:  
Characterization of new particle and secondary aerosol formation during summertime in Beijing,



976 China, *Tellus B: Chemical and Physical Meteorology*, 63:3, 382-394,  
977 <https://doi.org/10.1111/j.1600-0889.2011.00533.x>, 2011.

978  
979 Zhu, C., Li, J.G., Wang, L., Morawska, L., Zhang, X. and Zhang, Y.L.: Size-resolved particle  
980 distribution and gaseous concentrations by real-world road tunnel measurement, *Indoor and Built*  
981 *Environment*, 23, 2, 225-235, <https://doi.org/10.1177/1420326X13509290>, 2014.

982 **FIGURE CAPTIONS:**

983

984 **Figure 1.** Comparison of average particle number counts ( $\#/cm^3$ ) for nucleation, aitken,  
985 accumulation, large fine and coarse modes of PM between 15 nm and 10  $\mu m$  in all  
986 seasons, and the volume contributions for comparison.

987

988 **Figure 2.** Average diurnal variation of particle number counts for nucleation, Aitken,  
989 accumulation, large fine and coarse modes and  $PM_{2.5}$ , BC, NO and  $NO_2$  in autumn,  
990 summer and winter.

991

992 **Figure 3.** Average diurnal variation of total particle number counts (between 15 and 10  $\mu m$ ) for  
993 weekday average (Monday to Friday), Saturday and Sunday in Delhi. (Summer data  
994 are very limited. There are no data on Friday afternoon, night and Saturday early  
995 morning (Figure S6)).

996

997 **Figure 4.** Diurnal contour plots for particles derived by SMPS between 15 and 660 nm averaged  
998 for each season (a: winter, b: Autumn and c: Summer) and for 3 June 2018 data when  
999 a NPF event probably occurred (d), the solid line showing the  $NO_x$  mixing ratio. Note  
1000 the different scales for the seasons presented.

1001

1002 **Figure 5.** The hourly average of day and night particle numbers for all modes from the wide  
1003 range particle sizes derived from the merged data.  $UFP = \text{Nucleation} + \text{Aitken}$ ,  $PN_1 =$   
1004  $UFP + \text{Accumulation}$ ,  $PN_{10} = PN_1 + \text{Large Fine} + \text{Coarse}$ .

1005

1006 **Figure 6.** Seasonal average (line) and standard deviation (shadow) of particle number size  
1007 distributions.

1008

1009 **Figure 7.** Hourly average day and night (left side) and during day hours (right side) particle  
1010 number distributions in autumn, summer and winter in Delhi.

1011

1012 **Figure 8.** Diurnal change of the geometric mean diameter (GMD) calculated for winter, autumn  
1013 and summer seasons. Growth rates (nm/hour) are calculated from  $dGMD/dt$ .

1014

1015 **Figure 9.** Hourly average particle number, volume and area distributions in the winter (a),  
1016 autumn (b) and summer (c) in Delhi.

1017

1018 **Figure 10.** Correlation coefficient (R) between the hourly average PNs of five particle size  
1019 fractions (left side) and NO,  $NO_2$ , BC (right side).

1020

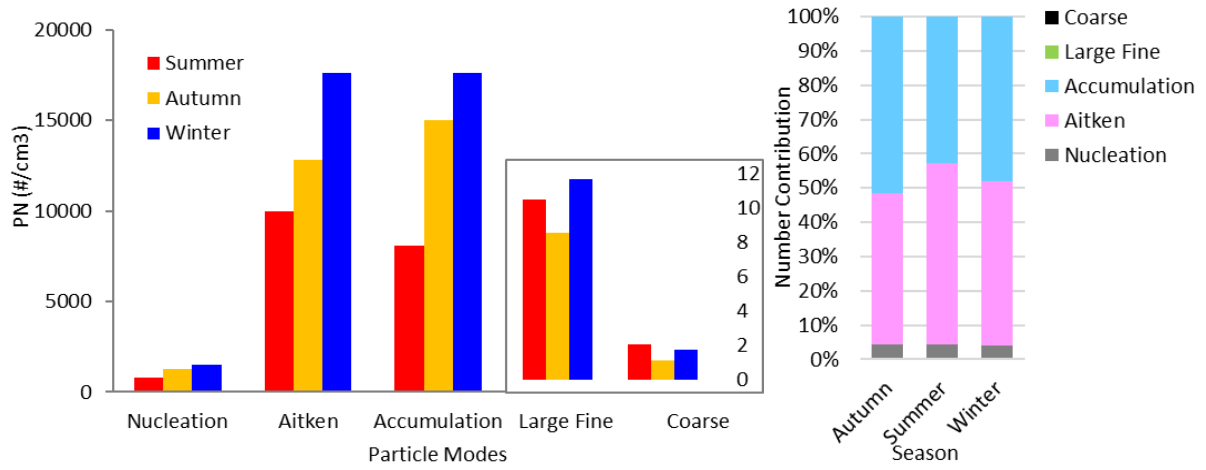
1021 **Figure 11.** Polar plots of PNs ( $\#/cm^3$ ) for five particle size fractions in winter, autumn and  
1022 summer in Delhi.

1023

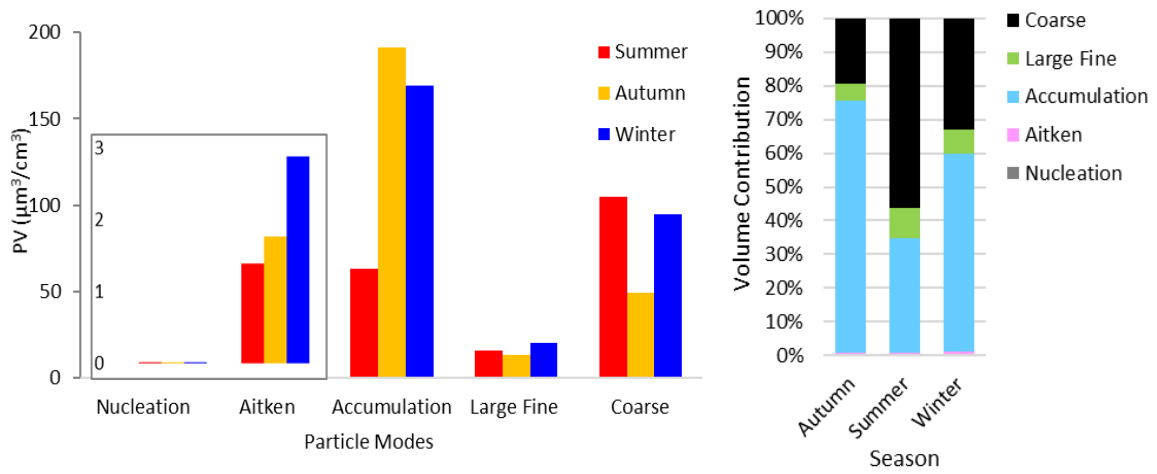
1024

1025

1026



1027



1028

1029

1030

1031

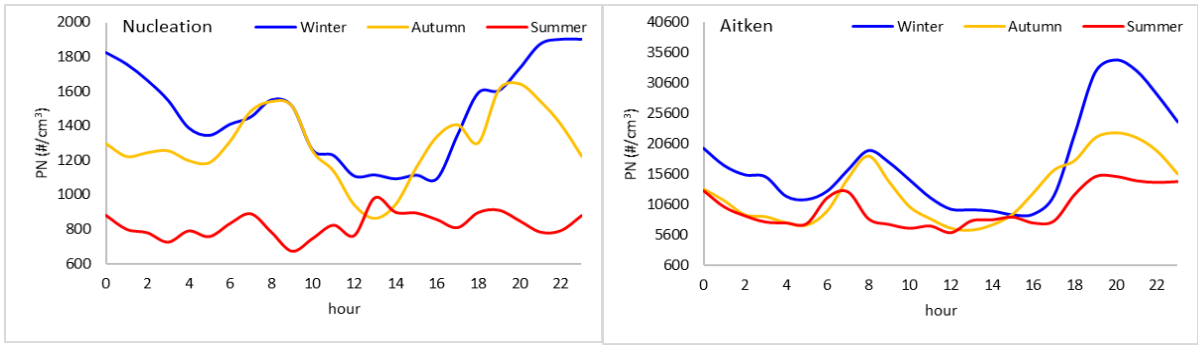
1032

1033

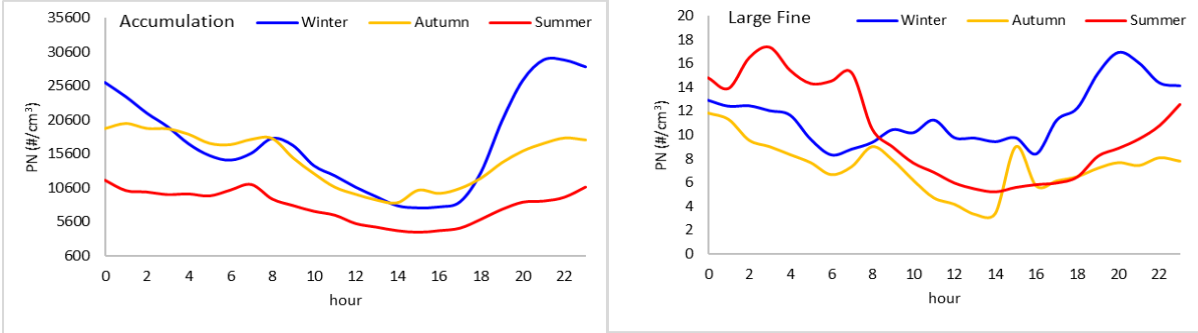
1034

**Figure 1.** Comparison of average particle number counts ( $\#/cm^3$ ) for nucleation, aitken, accumulation, large fine and coarse modes of PM between 15 nm and 10  $\mu m$  in all seasons, and the volume contributions for comparison.

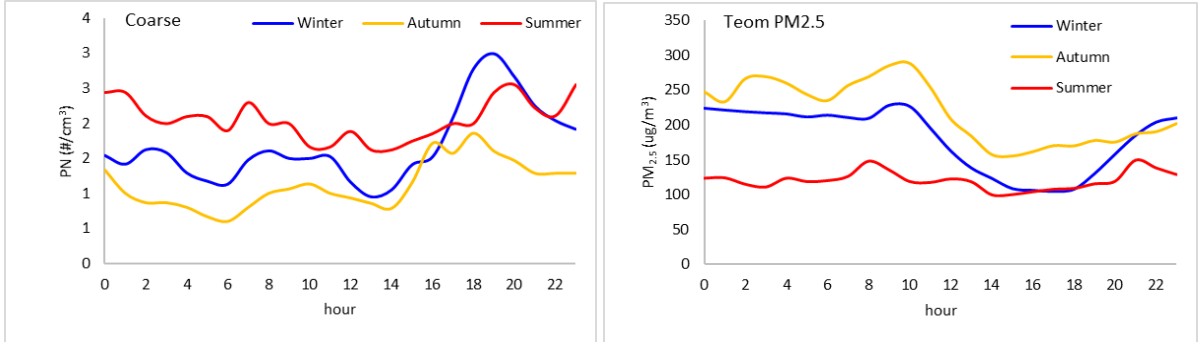
1035



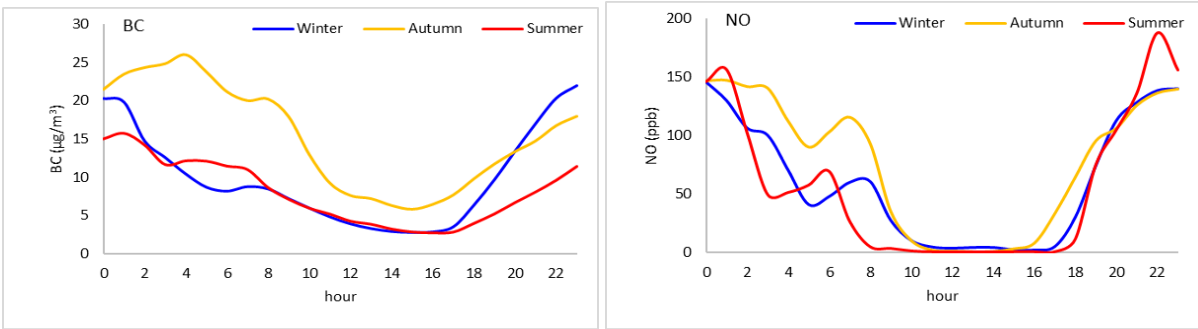
1036



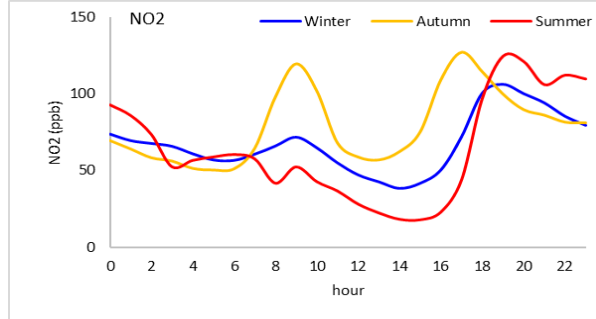
1037



1038



1039



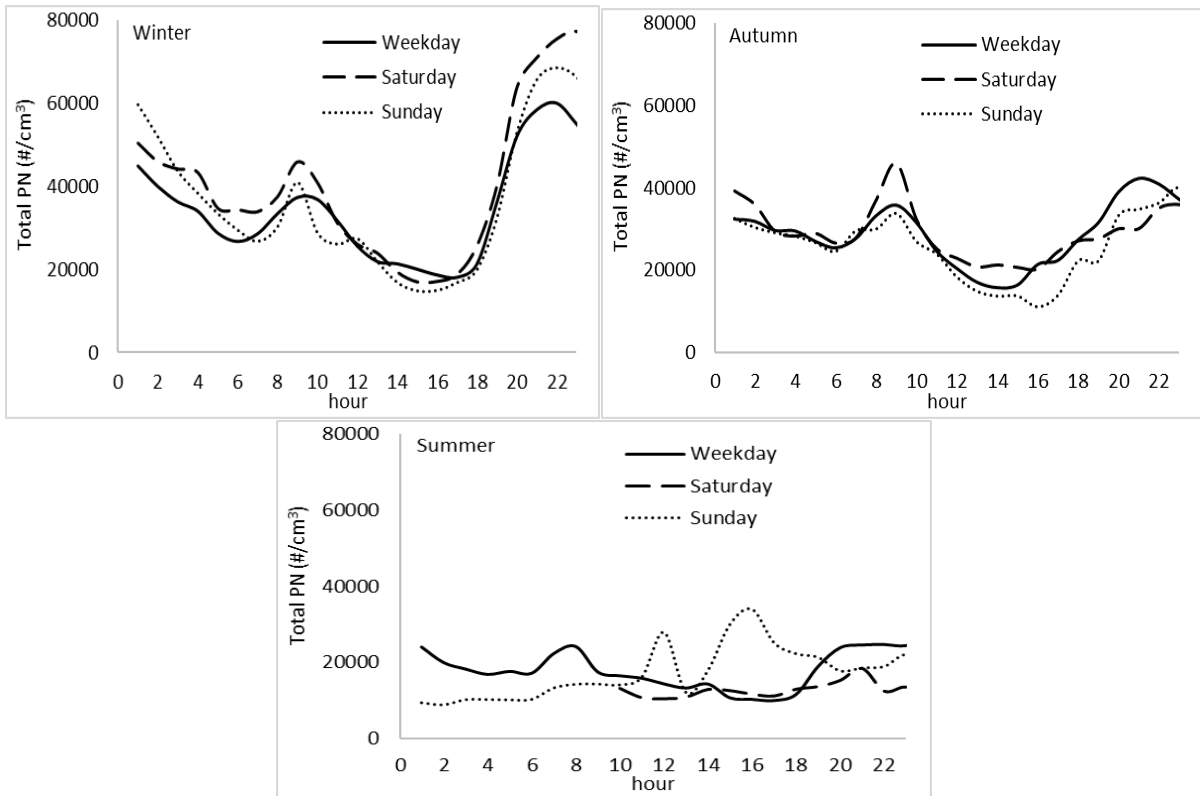
1040

1041

1042

**Figure 2.** Average diurnal variation of particle number counts for nucleation, Aitken, accumulation, large fine and coarse modes and PM<sub>2.5</sub>, BC, NO and NO<sub>2</sub> in autumn, summer and winter.

1043



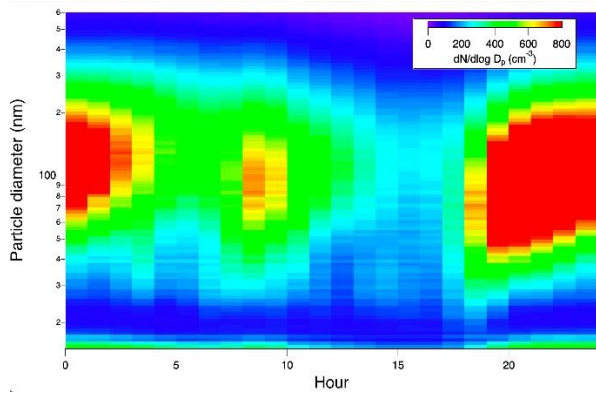
1044

1045

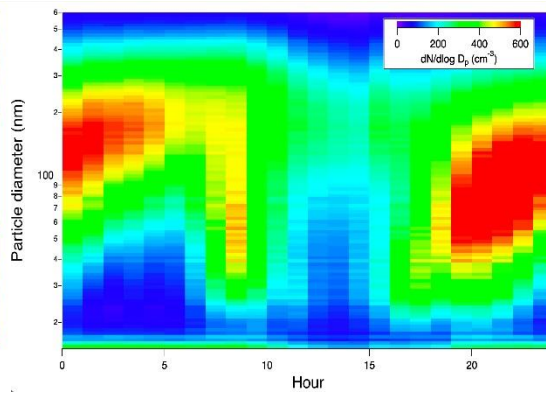
1046 **Figure 3.** Average diurnal variation of total particle number counts (between 15 and 10  $\mu\text{m}$ ) for  
1047 weekday average (Monday to Friday), Saturday and Sunday in Delhi. (Summer data are very  
1048 limited. There are no data on Friday afternoon, night and Saturday early morning (Figure S6)).  
1049

1050

1051



a) Winter

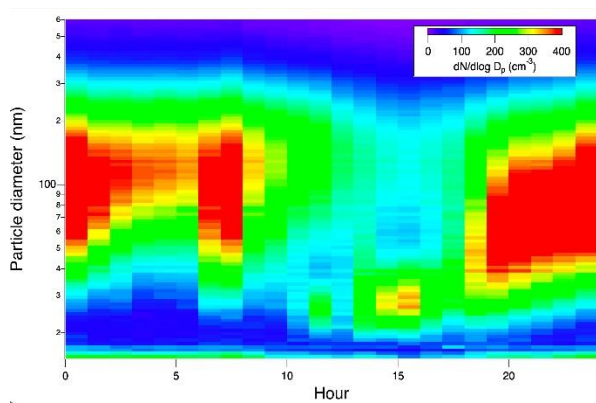


b) Autumn

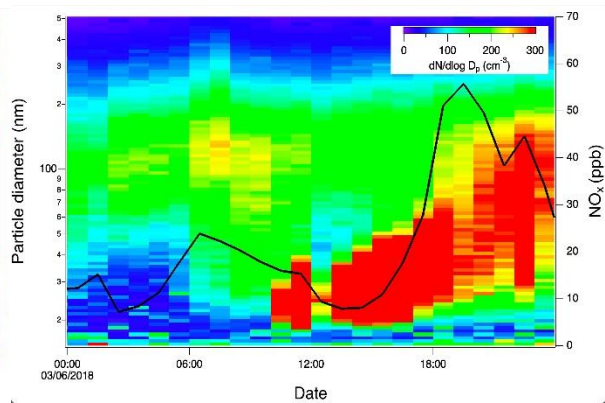
1052

1053

1054



c) Summer



d) 3 June 2018

1055

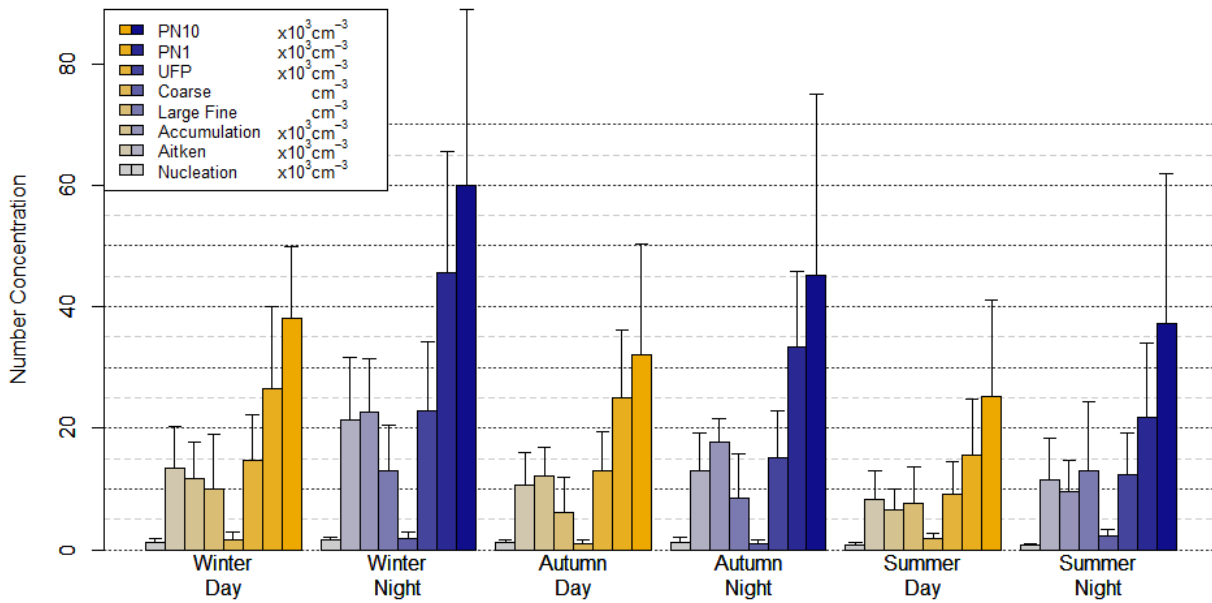
1056

1057

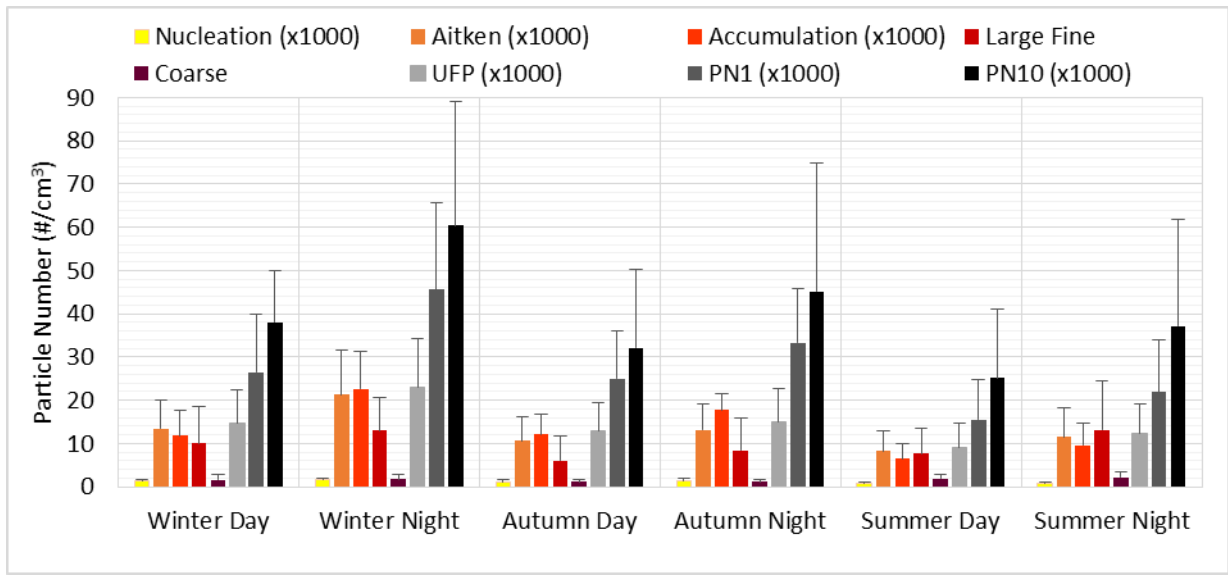
1058

1059

**Figure 4.** Diurnal contour plots for particles derived by SMPS between 15 and 660 nm averaged for each season (a: winter, b: Autumn and c: Summer) and for 3 June 2018 data when a NPF event probably occurred (d), the solid line showing the NO<sub>x</sub> mixing ratio. Note the different scales for the seasons presented.



1060



1061

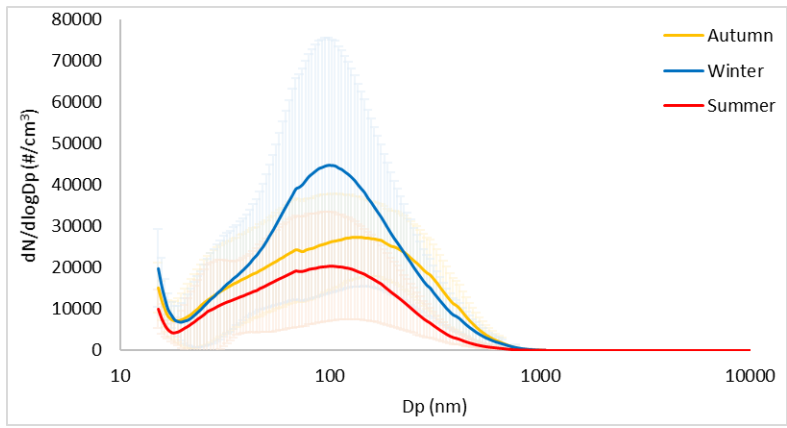
1062

1063

1064

1065

**Figure 5.** The hourly average of day and night particle numbers for all modes from the wide range particle sizes derived from the merged data. UFP =Nucleation +Aitken,  $PN_1 = \text{UFP} + \text{Accumulation}$ ,  $PN_{10} = PN_1 + \text{Large Fine} + \text{Coarse}$ .



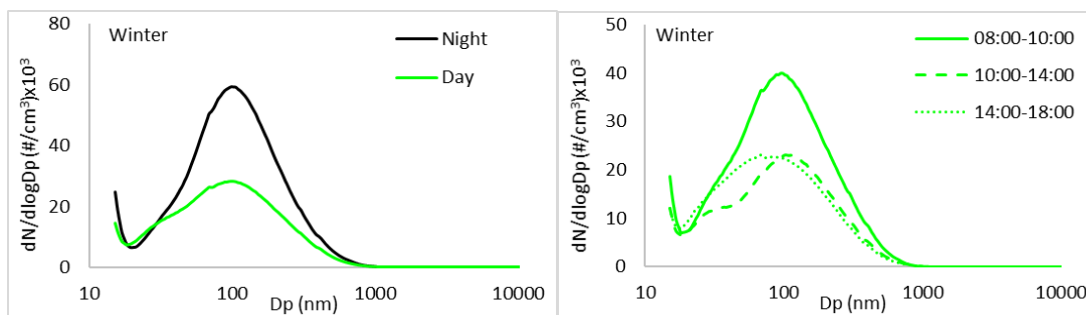
1066

1067 **Figure 6.** Seasonal average (line) and standard deviation (shadow) of particle number size  
1068 distributions.

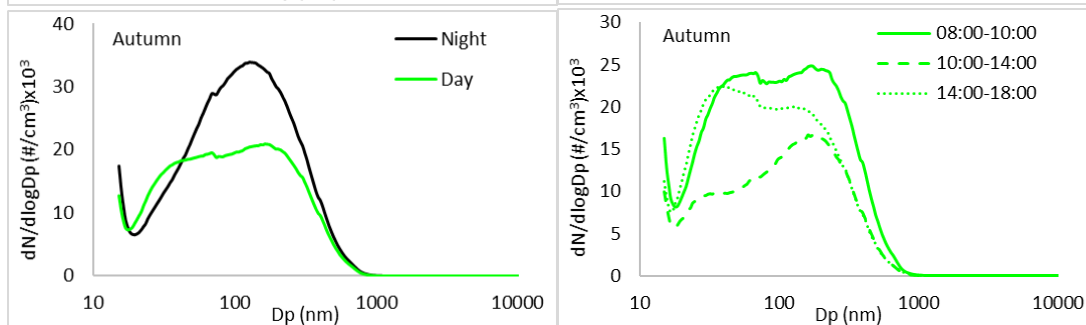
1069



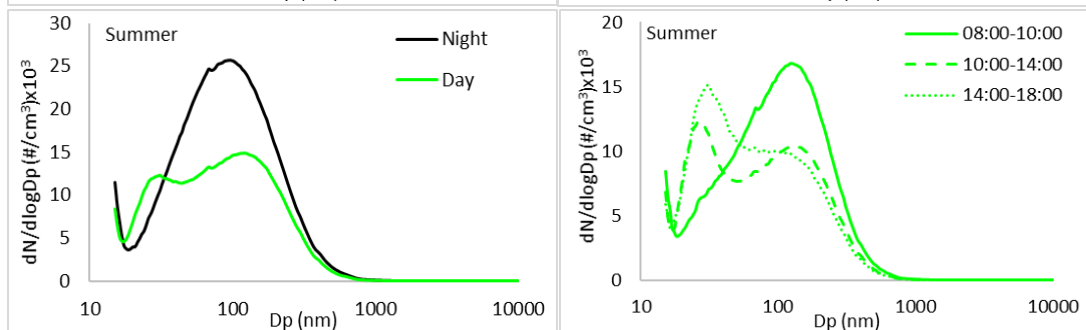
1070



1071



1072

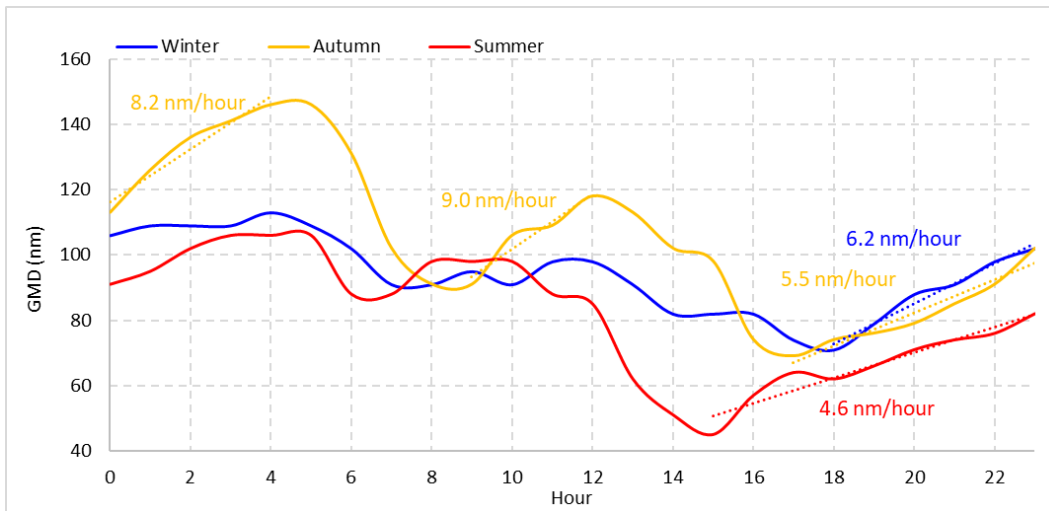


1073

1074

1075

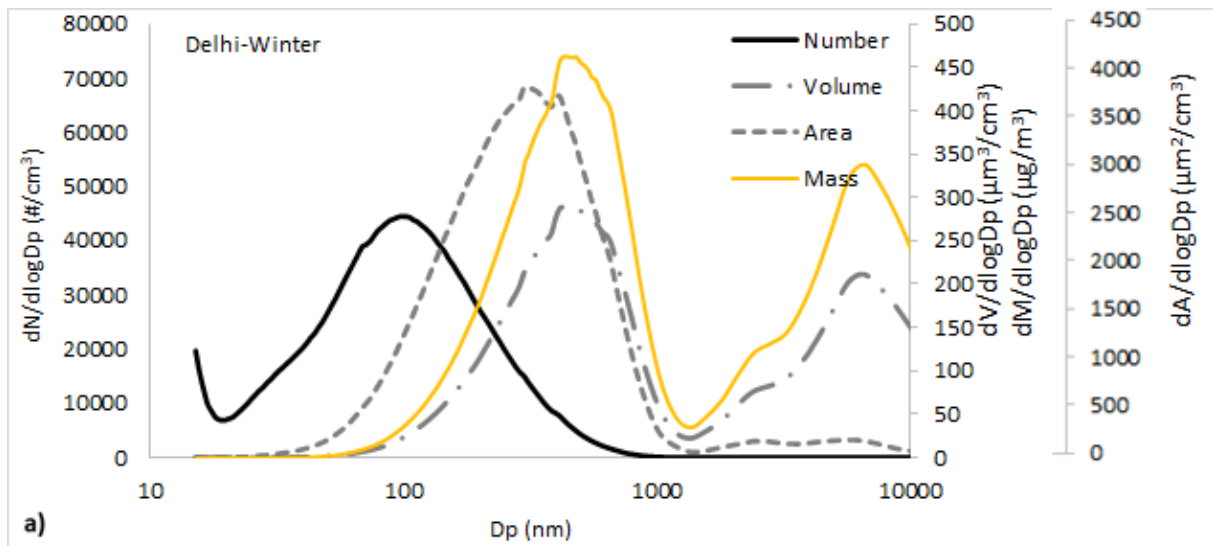
**Figure 7.** Hourly average day and night (left side) and during day hours (right side) particle number distributions in autumn, summer and winter in Delhi.



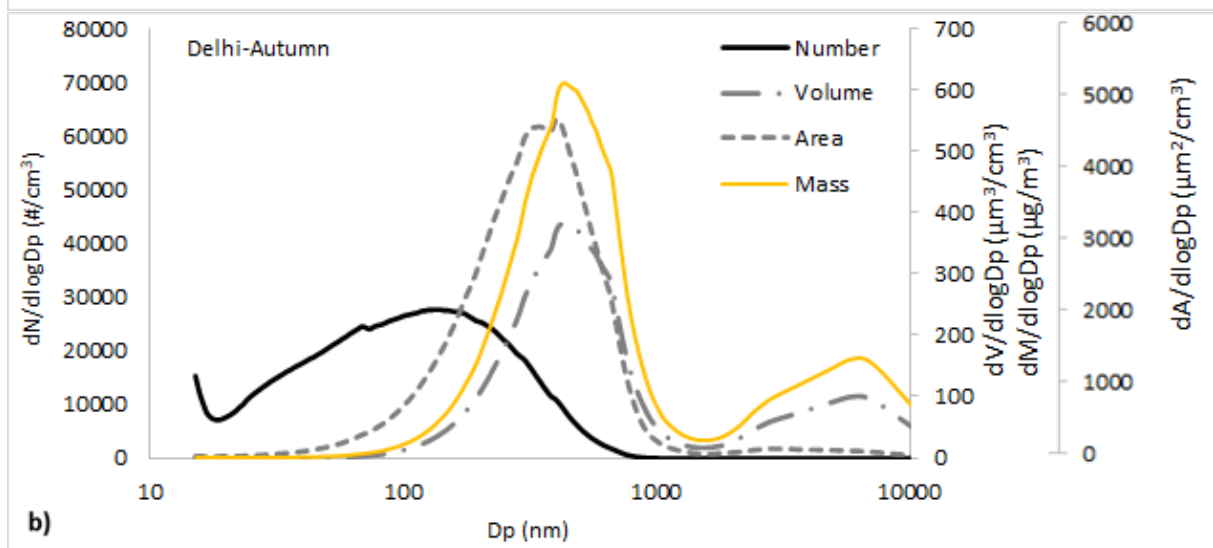
1076

1077 **Figure 8.** Diurnal change of the geometric mean diameter (GMD) calculated for winter, autumn  
 1078 and summer seasons. Growth rates (nm/hour) are calculated from  $dGMD/dt$ .  
 1079

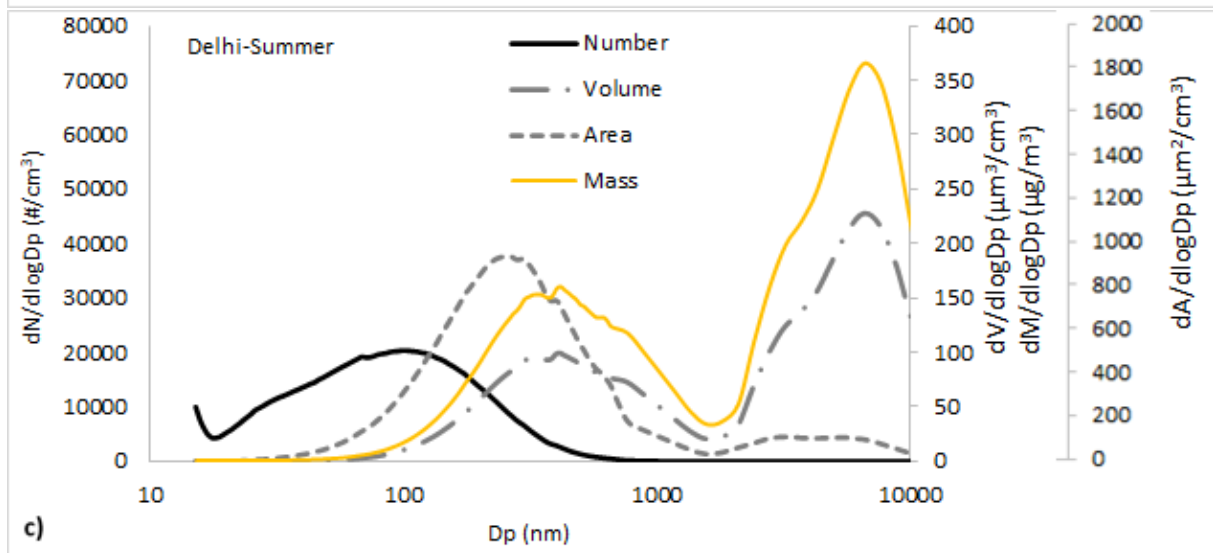
1080



1081



1082



1083 **Figure 9.** Hourly average particle number, volume and area distributions in the winter (a), autumn  
 1084 (b) and summer (c) in Delhi.  
 1085

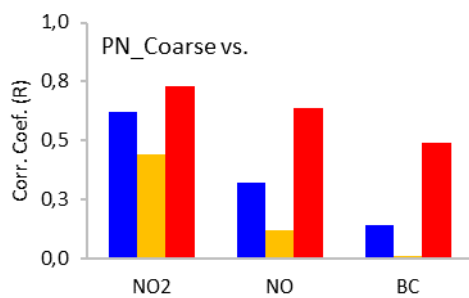
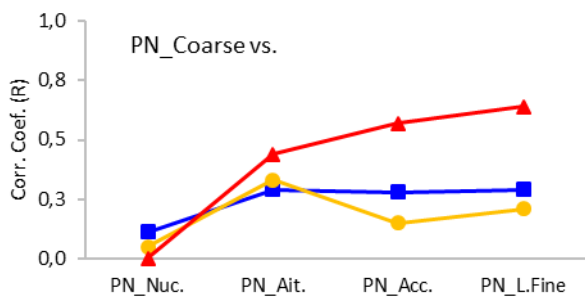
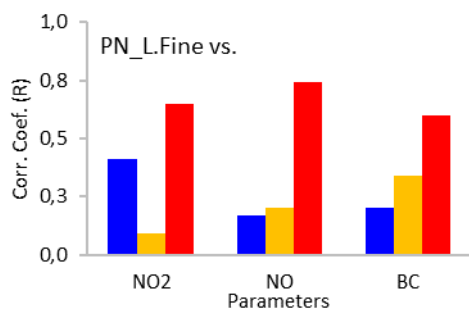
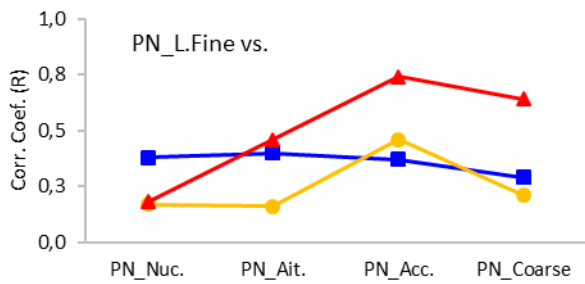
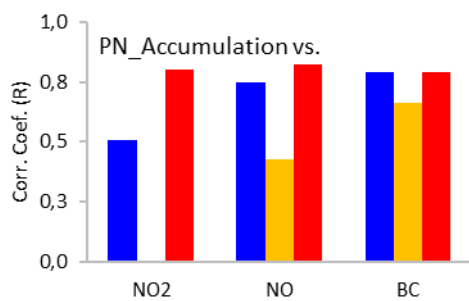
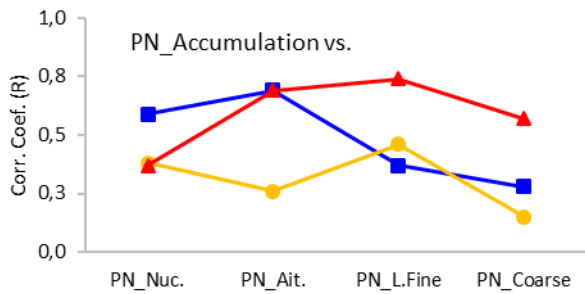
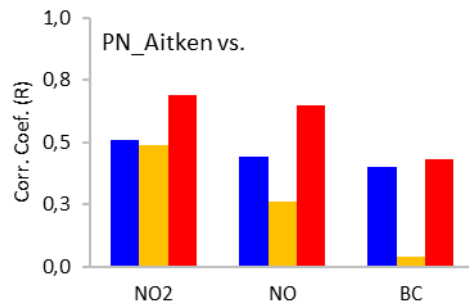
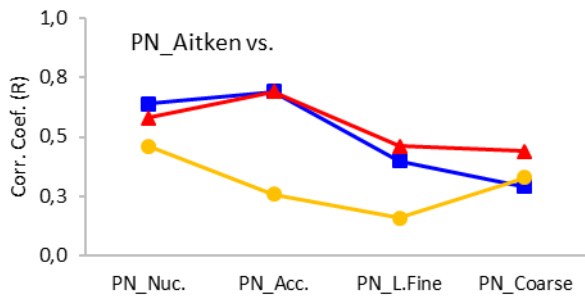
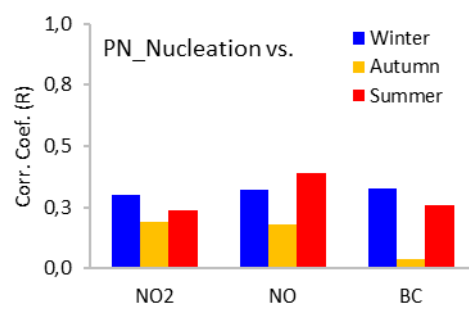
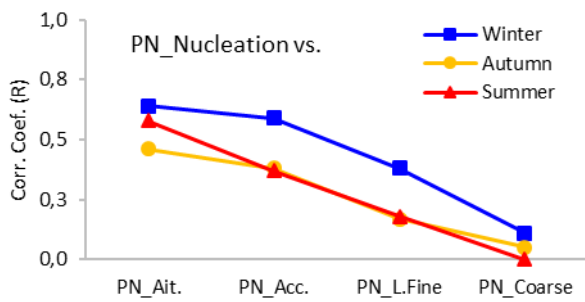
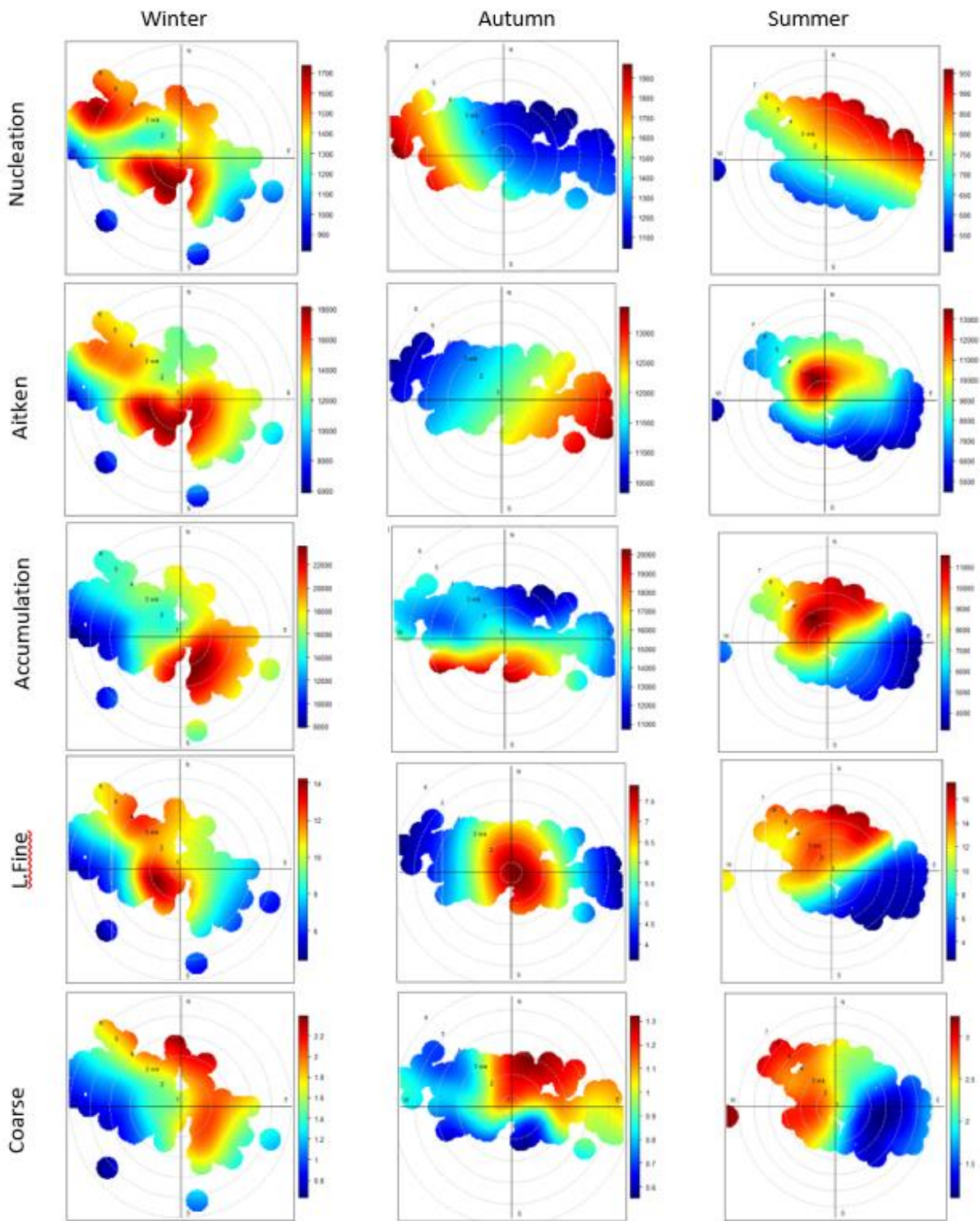


**Figure 10.** Correlation coefficient (R) between the hourly average PNs of five particle size fractions (left side) and NO, NO<sub>2</sub>, BC (right side).



1095

1096

1097

1098

1099

**Figure 11.** Polar plots of PNs ( $\#/cm^3$ ) for five particle size fractions in winter, autumn and summer in Delhi.